

# The Metal Contents of Very Low Column Density Lyman-alpha Clouds: Implications for the Origin of Heavy Elements in the Intergalactic Medium<sup>1</sup>

Limin Lu<sup>2</sup>, Wallace L. W. Sargent<sup>2</sup>, Thomas A. Barlow<sup>3</sup>, and Michael Rauch<sup>2,4</sup>

## ABSTRACT

We investigate the metal contents of Ly $\alpha$  clouds at  $2.2 < z < 3.6$  with  $10^{13.5} < N(\text{H I}) < 10^{14} \text{ cm}^{-2}$  using high resolution, high S/N spectra of 9 quasars obtained with the 10m Keck I telescope. Previous investigations of similar nature were limited to Ly $\alpha$  clouds with  $N(\text{H I}) > 10^{14.5} \text{ cm}^{-2}$  for which a mean metallicity of  $[\text{C}/\text{H}] \simeq -2.5$  was deduced. It has been suggested that the metals seen in these clouds may have been produced by a generation of Population III stars occurred at a much earlier epoch before the formation of quasars and normal galaxies. We shift the quasar spectra into the rest frame of each Ly $\alpha$  cloud with  $10^{13.5} < N(\text{H I}) < 10^{14} \text{ cm}^{-2}$  and then average the rest-frame spectra in the spectral region encompassing the C IV  $\lambda\lambda 1548.20, 1550.77$  absorption lines in order to vastly improve the S/N of the final composite spectrum.

After eliminating a small number of Ly $\alpha$  lines that are estimated to have  $10^{13.5} < N(\text{H I}) < 10^{14} \text{ cm}^{-2}$  which individually show detectable C IV absorption, the remaining  $\sim 300$  lines whose corresponding C IV  $\lambda 1548.20$  regions are clean are divided into various samples to form composite spectra. No significant C IV absorption is detected in any of the composite spectra we investigated. We derive an upper limit of  $< 0.088 \text{ m}\text{\AA}$  (95.5% confidence limit) for the equivalent width of the C IV  $\lambda 1548.20$  line, corresponding to  $[\text{C}/\text{H}] < -3.5$  using the cosmological simulations of Rauch, Haehnelt, & Steinmetz (1997) to infer the ionization correction; the same simulation results have been used to deduce a mean metallicity of  $[\text{C}/\text{H}] \simeq -2.5$  for Ly $\alpha$  clouds with  $N(\text{H I}) > 10^{14.5} \text{ cm}^{-2}$ .

The mean metallicities of Ly $\alpha$  clouds with  $10^{13.5} < N(\text{H I}) < 10^{14} \text{ cm}^{-2}$ ,  $[\text{C}/\text{H}] < -3.5$ , is a factor of 10 lower than that inferred for Ly $\alpha$  clouds with  $N(\text{H I}) > 10^{14.5} \text{ cm}^{-2}$ . This suggests that a sharp drop in the metallicity level of the intergalactic gas sets in at  $10^{14} < N(\text{H I}) < 10^{14.5} \text{ cm}^{-2}$ . The result rules out the suggestion that a generation of Pop III stars could have polluted the entire universe

---

<sup>1</sup>Based on observations obtained at the W. M. Keck observatory, which is jointly operated by the California Institute of Technology and the University of California.

<sup>2</sup>California Institute of Technology, 105-24, Pasadena, CA 91125

<sup>3</sup>California Institute of Technology, 100-22, Pasadena, CA 91125

<sup>4</sup>Hubble Fellow

to a (nearly) uniform metallicity level of  $[C/H] \simeq -2.5$ . Cosmological simulations involving gas hydrodynamics indicate that Ly $\alpha$  clouds with  $N(\text{H I}) > 10^{14.5} \text{ cm}^{-2}$  mostly occur in the filamentary gaseous regions surrounding and connecting collapsed objects, while those with  $N(\text{H I}) < 10^{14} \text{ cm}^{-2}$  are preferentially found in void regions further away from collapsed structures. These results, coupled with the simulation results of Ostriker & Gnedin (1996) and Gnedin & Ostriker (1997) for Pop III star formation and enrichment, strongly suggest that most of the heavy elements in Ly $\alpha$  clouds with  $N(\text{H I}) > 10^{14.5} \text{ cm}^{-2}$  (i.e., gas in the filaments) were probably produced *in situ* by Pop II stars, in the sense that they were either made by stars within the clouds or were ejected from nearby star-forming galaxies. Within this context, clouds with  $N(\text{H I}) < 10^{14} \text{ cm}^{-2}$  (i.e., gas in the void regions) may only have experienced pollution from Pop III stars.

We derive constraints on the metallicities of the small number of Ly $\alpha$  clouds with  $10^{13.5} < N(\text{H I}) < 10^{14} \text{ cm}^{-2}$  that individually show detectable C IV absorption and discuss their possible nature.

*Subject headings:* galaxies: intergalactic medium - quasars: absorption lines

## 1. INTRODUCTION

The Ly $\alpha$  forest clouds seen in spectra of quasars, which are crudely defined to have  $N(\text{H I}) < 10^{16} - 10^{17} \text{ cm}^{-2}$ , were thought initially to contain primordial gas since no metal absorption lines were detected at their redshifts (Sargent et al 1980). However, moderate-resolution spectra taken with much higher S/N ratios (Meyer & York 1987) provided the first evidence that some of these clouds, especially those with relative large equivalent width, do show weak C IV absorption. By shifting to the rest frame and averaging the C IV regions of hundreds of Ly $\alpha$  lines which did not show C IV absorption individually, Lu (1991) provided a probable detection of C IV absorption associated with these clouds at the  $w_r(1548) \sim 7 \text{ m}\text{\AA}$  level. Subsequent high resolution, high S/N spectra taken with the 10m Keck telescopes (Cowie et al 1995; Tytler et al 1995; Songaila & Cowie 1996) have clearly revealed (mostly) weak C IV absorption associated with individual Ly $\alpha$  clouds at  $z \sim 3$  with  $N(\text{H I})$  as low as  $10^{14.5} \text{ cm}^{-2}$ . Specifically, it was found that essentially all clouds with  $N(\text{H I}) \geq 10^{15} \text{ cm}^{-2}$  show C IV absorption, and that 50-75% of the Ly $\alpha$  clouds with  $N(\text{H I}) \geq 10^{14.5} \text{ cm}^{-2}$  show C IV absorption.

The presence of C IV absorption in Ly $\alpha$  clouds with  $N(\text{H I}) > 10^{14.5} \text{ cm}^{-2}$  indicates that these clouds have been enriched in heavy elements at redshifts as high as  $z > 3.6$ . Recent cosmological simulations of structure formation involving gas processes (hydrodynamics) suggest that the Ly $\alpha$  lines at  $z > 2$  represent low density gas in-between collapsed objects and are closely related to the formation of galaxies, clusters, voids, and other structures in the universe (Cen et al 1994; Petitjean, Mucket, & Kates 1995; Zhang, Anninos, & Norman 1995; Hernquist et al 1996;

Miralda-Escude et al 1996). An important issue is whether the metals seen in these intergalactic clouds were produced locally (i.e., produced by stars formed within the clouds, or ejected from nearby star-forming galaxies) or were produced at a much earlier epoch in a wide-spread fashion (i.e., by Population III stars; Ostriker & Gendin 1996).

If the metals in Ly $\alpha$  clouds were produced *in situ*, one may expect that clouds in regions of space sufficiently far away from star-forming objects should be metal-free. Whereas in the case of Pop III star enrichment, most of the universe may have been polluted to some degree and few clouds may be entirely metal-free. While it is not yet possible to directly see the spatial distributions of star-forming objects and Ly $\alpha$  clouds at high redshift, some insight is provided by cosmological simulations. These simulations indicate that clouds with  $10^{14.5} < N(\text{H I}) < 10^{17} \text{ cm}^{-2}$  account for 40-60 % of the total baryons in the universe at  $z = 2 - 4$  (Miralda-Escude et al 1996), and that such clouds preferentially occupy the filamentary gaseous regions surrounding and connecting collapsed structures (i.e., galaxies). The simulations also indicate that clouds with  $N(\text{H I}) < 10^{14} \text{ cm}^{-2}$  predominantly occupy the void regions. These results lead to the idea that one can perhaps obtain clues about the origin of the metals by investigating the metal contents of the very low column density (i.e.,  $N(\text{H I}) < 10^{14} \text{ cm}^{-2}$ ) clouds: the presence of any significant amount of metals in these clouds would favor the Pop III idea for the reasons discussed above.

In this paper we present the results of a search for C IV absorption associated with Ly $\alpha$  clouds with  $10^{13.5} < N(\text{H I}) < 10^{14} \text{ cm}^{-2}$ , using high resolution, high S/N quasar spectra obtained with the 10m Keck I telescope and the High Resolution Spectrometer (HIRES; Vogt 1992). Given the low  $N(\text{H I})$  of the clouds, it would be practically impossible to obtain spectra of quasars with sufficient S/N to detect the C IV absorption in individual clouds even if the  $N(\text{C IV})/N(\text{H I})$  ratio remains the same as that in clouds with higher  $N(\text{H I})$  (S/N at least a factor of 5 better than the current best spectrum would be required). The problem is compounded by the fact that the  $N(\text{C IV})/N(\text{H I})$  ratio is predicted to drop with decreasing  $N(\text{H I})$  at  $N(\text{H I}) < 10^{14} \text{ cm}^{-2}$  as the clouds become more ionized (e.g. Rauch, Haehnelt, & Steinmetz 1997). Accordingly, the technique we adopt is the composite spectrum method pioneered by Norris, Hartwick, & Peterson (1983). Essentially, one shifts a quasar spectrum into the rest frame of each Ly $\alpha$  absorption line and then averages the rest-frame spectra over the spectral region encompassing the C IV  $\lambda\lambda 1548.20, 1550.77$  lines to form a composite spectrum. The S/N in the composite spectrum increases roughly as the square root of the number of lines being averaged, making this a very effective way to achieve ultra-high S/N without using unrealistically large amounts of telescope time. The end result is then an average C IV absorption associated with an ensemble of Ly $\alpha$  clouds. This technique has been applied previously to Ly $\alpha$  clouds to search for C IV absorption by Williger et al (1989), Lu (1991), Tytler & Fan (1994), and Barlow & Tytler (1998), and to metal systems to search for O VI absorption by Lu & Savage (1993). Incidentally, this averaging process automatically suppresses any residual noise features in the spectra caused by imperfect flatfielding or other artifacts and is ideal for achieving ultra-high S/N in the averaged spectra.

In section 2 we describe the spectra used in the analysis and the procedure for selecting Ly $\alpha$

lines with the desired column densities (i.e.,  $10^{13.5} < N(\text{H I}) < 10^{14} \text{ cm}^{-2}$ ). The composite spectra for various samples of Ly $\alpha$  clouds are discussed in section 3. No C IV absorption is detected in any of the composite spectra, thus yielding only upper limits to the metallicity of the clouds. In section 4 we discuss the implications of our results for the nature of the metal enrichment in the Ly $\alpha$  clouds. We briefly summarize our main conclusions in section 5.

## 2. THE Ly $\alpha$ LINE SAMPLE

### 2.1. Selection of Ly $\alpha$ Lines

The list of 9 quasars whose spectra are used in the analyses is given in Table 1. These objects are selected because their spectra have the highest S/N among all  $z_{em} > 2.5$  quasars observed by the current authors with the Keck HIRES. The objects have emission redshifts between 2.58 to 3.63. The integration times range from 4 to 11 hours. The data were reduced using the EE package developed by T. Barlow. The typical S/N per resolution element ( $6.6 \text{ km s}^{-1}$ ) in the C IV region for each spectrum is given in the 4th column of Table 1.

Our goal is to determine the metallicity of Ly $\alpha$  clouds with  $N(\text{H I})$  in the range of  $10^{13.5}$  to  $10^{14} \text{ cm}^{-2}$  via the C IV  $\lambda\lambda$  1548.20, 1550.77 absorption. Such clouds could be selected by fitting Voigt profiles to all the Ly $\alpha$  lines in the spectra as is commonly done. Since such profile fitting has not been done to all of the spectra listed in Table 1 and indeed would be quite time consuming to carry out, we instead selected Ly $\alpha$  lines in the desired column density range based on the observed depth of the lines at the line center. Previous Voigt profile fitting to Ly $\alpha$  forest absorption lines obtained with the Keck HIRES indicate that the Doppler width distribution of the Ly $\alpha$  lines at  $2 < z < 4$  is sharply peaked at  $b \simeq 25 \text{ km/s}$  with the vast majority of lines having  $b$  between 20 and  $50 \text{ km s}^{-1}$  (Hu et al 1995; Lu et al 1996a; Kirkman & Tytler 1997). For a mean  $b = 25 \text{ km s}^{-1}$ , the central optical depths corresponding to the limiting  $N(\text{H I})$  of  $10^{13.5}$  and  $10^{14} \text{ cm}^{-2}$  are 0.96 and 3.03. The corresponding absorption lines should have a residual flux between 0.384 and 0.048 at the line center for unity continuum (note that the lines are completely resolved at the HIRES resolution of  $\text{FWHM} = 6.6 \text{ km s}^{-1}$  for the assumed  $b$  value). We therefore selected Ly $\alpha$  clouds with  $10^{13.5} < N(\text{H I}) < 10^{14} \text{ cm}^{-2}$  by visually selecting Ly $\alpha$  lines with residual flux between 0.384 and 0.048 after normalizing the spectrum to unity continuum.<sup>5</sup> In order to avoid biasing the line sample, only spectral regions which have sufficiently high S/N to securely identify absorption lines with residual flux of 0.048 were used. The spectral regions actually used to select Ly $\alpha$  lines are given in column 5 of Table 1. The lower wavelength limit is determined either by the above S/N requirement or by the onset of Ly $\beta$  emission of the quasar (we do not use the spectral region shortward of Ly $\beta$  emission in order to avoid mis-identifying Ly $\beta$  and higher order Lyman lines

---

<sup>5</sup>Some of the spectra contain damped Ly $\alpha$  absorption lines (cf. Wolfe 1988). In such cases, the adopted continua take into account the wings of the damped Ly $\alpha$  absorption.

with Ly $\alpha$ ). The upper wavelength limit is determined by the Ly $\alpha$  emission.

In many cases Ly $\alpha$  lines with the desired optical depth (i.e., residual flux between 0.384 and 0.048) are blended with other lines. If the blending is severe enough, two problems arise: (1) the blending makes it difficult to determine an accurate redshift for the absorption line; (2) the blending could lead to a significant overestimate of the H I column density of the absorption lines. To avoid these problems, we excluded from the sample Ly $\alpha$  lines within 50 km s<sup>-1</sup> of other “strong” lines (Ly $\alpha$  or something else) that would have otherwise been included in the sample. A “strong” line is defined here to have residual flux < 0.384 (i.e., N(H I) > 10<sup>13.5</sup> cm<sup>-2</sup> if it is a Ly $\alpha$ ). The choice of 50 km s<sup>-1</sup> is somewhat arbitrary and is based on the observation that Ly $\alpha$  lines satisfying the above criterion do appear to have well-defined redshifts and largely fall into the desired column density range. It is important to emphasize that, while it is critical for the line sample to be unbiased with respect to the column density distribution so that the average N(H I) of the lines comes out to be what is expected (see below), it is not necessary for the line sample to be complete.

Most of the metal lines occurring in the Ly $\alpha$  forest are easy to recognize owing to their narrow line width (see, for example, Kirkman & Tytler 1997). Relatively broad metal lines that are strong enough to be mistaken as Ly $\alpha$  lines in the desired column density range are rare and are also easy to identify because they are usually associated with prominent metal systems. Spectral regions that are severely affected by metal absorption lines were not used to search for Ly $\alpha$  lines. There are a few cases where the presumed Ly $\alpha$  lines have estimated width of 15 <  $b$  < 18 km s<sup>-1</sup>, which could be Ly $\alpha$  lines but could also be unidentified metal lines; these are assumed to be Ly $\alpha$  lines. Since the number of such lines is very small (< 5%), their effect on the final composite spectrum and on the interpretation should be negligible.

The selection criteria we employed will occasionally include some Ly $\alpha$  lines with N(H I) outside the range of 10<sup>13.5</sup> – 10<sup>14</sup> cm<sup>-2</sup> and exclude some other Ly $\alpha$  lines within the desired column density range if the actual Doppler widths of the lines are significantly different from the assumed mean of 25 km s<sup>-1</sup>. For example, a line with  $b = 15$  km s<sup>-1</sup> and residual flux 0.384 (i.e., barely strong enough to be included in the sample if it had  $b = 25$  km s<sup>-1</sup>) would have N(H I) = 10<sup>13.28</sup> cm<sup>-2</sup> but would still be included in the sample. On the other hand, a line with  $b = 50$  km s<sup>-1</sup> and residual flux 0.3 would have a N(H I) = 10<sup>13.80</sup> cm<sup>-2</sup> and would be excluded from the sample. However, because of the sharpness of the Doppler distribution of the Ly $\alpha$  clouds, and because of the range of column densities considered, the vast majority of lines in the sample should have the desired N(H I) values. The only major effect of the above “shuffling” is to broaden the column density distribution of the selected lines. The mean N(H I) of the sample should be largely unaffected.

Kirkman & Tytler (1997) have fitted Voigt profiles to all Ly $\alpha$  lines in the HIRES spectrum of Q1946+7658 which they took independently. It is therefore possible to examine the actual N(H I) distribution of the Ly $\alpha$  lines in the Q1946+7658 spectrum that are included in our sample

based on the above selection criteria using the results of Kirkman & Tytler. Figure 1 shows this  $N(\text{H I})$  distribution for the 47 systems which we have selected based on their optical depth. As expected, some of the systems (9/47 or 19%) have  $N(\text{H I})$  outside the desired range, and the extremes are  $N(\text{H I}) = 10^{13.26}$  and  $10^{14.10} \text{ cm}^{-2}$ . The average  $N(\text{H I})$  of the 47 Ly $\alpha$  lines included in the sample for Q1946+7658 is  $10^{13.783} \text{ cm}^{-2}$  based on the profile fitting results. The expected mean column density from the column density distribution,  $f(N) \propto N^{-1.5}$  (Hu et al 1995; Lu et al 1996a; Kirkman & Tytler 1997), is  $10^{13.750} \text{ cm}^{-2}$ . Note that the mean  $N(\text{H I})$  is extremely robust. For example, if the power law index is 1.4 rather than 1.5 as assumed, the expected mean  $N(\text{H I})$  becomes  $10^{13.755}$ . The robustness of the mean  $N(\text{H I})$  has to do with the fact that the total column density range considered here spans only a factor of 3. The true mean  $N(\text{H I})$  of any given sample will fluctuate according to the sample size. Most of the samples we consider here (Table 4) contain between 126 and 282 lines. Monte Carlo simulations indicate that the  $1\sigma$  dispersion in the mean  $N(\text{H I})$  for samples of such sizes ranges between 0.006 and 0.013 dex for the assumed  $N(\text{H I})$  distribution. The  $1\sigma$  dispersion in the mean  $N(\text{H I})$  for the sample with 27 lines is 0.028 dex, and that for the sample containing 12 lines is 0.04 dex. These uncertainties are very small. The uncertainties associated with the mean  $N(\text{H I})$  of the actual samples will be somewhat larger than what the simulations indicate because of the “shuffling” effect discussed above. Even so, the uncertainties associated with the mean  $N(\text{H I})$  should be small compared to other uncertainties involved in the analysis (e.g., the ionization correction). We therefore believe that the simple selection procedure employed above does form a sample of Ly $\alpha$  lines with the vast majority of them having the desired range in  $N(\text{H I})$ , and that the average  $N(\text{H I})$  of the sample is unbiased and can be estimated reliably from the known column density distribution. Finally, we note that while line blending and blanketing effects can bias the observed  $N(\text{H I})$  distribution of Ly $\alpha$  clouds, such biases are apparently negligible at the column densities we consider here (see Kirkman & Tytler 1997, for example).

## 2.2. Individual Ly $\alpha$ Systems with C IV Absorption

Before we formed the composite spectrum, we visually examined the C IV region of individual Ly $\alpha$  systems in the sample to see if any of them have detectable C IV absorption in the observed spectra. Sixteen such systems were found, 6 of which form 3 close pairs ( $\Delta v < 50 \text{ km s}^{-1}$ ) and may be physically related. Three of the 16 systems are marginal in the sense that only weak ( $4 - 6\sigma$ ) C IV  $\lambda 1548$  absorption is detected and the corresponding  $\lambda 1550$  absorption is not apparent. We show in Figure 2 these Ly $\alpha$  lines and the corresponding C IV absorption. The properties of these systems are summarized in Table 3 and are discussed in more detail in section 4.2. These systems will be excluded from the composite spectrum analyses.

Nine of the 16 systems with detected C IV occur within  $3,000 \text{ km s}^{-1}$  of the Ly $\alpha$  emission redshift of the quasars. It has been known for some time that there is in general an excess of metal absorption systems near  $z_{em}$  of quasars, which are likely associated with material ejected

from the quasar nuclei or in the host galaxies and their environment (cf. Foltz et al 1988). We therefore classify these 9 systems as “associated” systems in Table 3. The remaining 7 systems are more than  $10,000 \text{ km s}^{-1}$  away from the  $\text{Ly}\alpha$  emission redshift of the background quasars; these are classified as “intervening” in Table 3.

Most of the systems listed in Table 3 show no detectable Si IV absorption except for the two pairs of associated systems at  $z = 3.62$  toward Q 1422+2309 and at  $z = 2.56$  toward Q 2343+1232, which happen to have (perhaps not by accident) the strongest C IV absorption among all systems given in Table 3. The  $z = 3.45129$  system toward Q 1422+2309 has a marginally significant Si IV  $\lambda 1393$  absorption without obvious  $\lambda 1402$  absorption.

Of the 7 intervening systems, 4 are within  $500 \text{ km s}^{-1}$  of other C IV absorption systems, while another one is within  $800 \text{ km s}^{-1}$  of other C IV systems (see figure 2). Interestingly, the 2 systems that do not have other C IV absorption systems within  $1000 \text{ km s}^{-1}$ , the  $z = 3.31822$  system toward Q1422+2309 and the  $z = 2.50221$  system toward Q2343+1232, are both marginal in their C IV detection. These results suggest a possible trend that low  $N(\text{H I})$   $\text{Ly}\alpha$  clouds are more likely to show metal absorption when they are close to other metal systems. This possibility is explored later in section 3. The 2 marginal systems that do not have other metal systems within  $1000 \text{ km s}^{-1}$  could be false identifications.

### 3. COMPOSITE SPECTRA AND MEASUREMENTS

#### 3.1. Composite Spectrum

Before we formed the composite spectrum, we visually inspected the spectral region of each quasar between the  $\text{Ly}\alpha$  and C IV emission lines and masked out any features (absorption lines, apparent emission features due to cosmic rays, features due to poor subtraction of night sky lines or telluric absorption lines, etc) that deviate significantly from the continuum. This essentially removed all features with significance above  $\sim 2\sigma$  level (as judged by eye). We will refer to these masked-out regions as “bad” regions or regions containing “bad pixels”, and refer to the resulting spectra as “cleaned spectra”. The bad regions are excluded from entering into the composite spectra.

We then examined the C IV region corresponding to each  $\text{Ly}\alpha$  line in the sample in the cleaned spectra, and assign a flag to each system according to the “cleanness” of its C IV region: “0” for systems whose C IV  $\lambda\lambda 1548.20, 1550.77$  regions are both clean, “1” for systems whose  $\lambda 1550.77$  region is clean but whose  $\lambda 1548.20$  region contains bad pixels, “2” for systems whose  $\lambda 1548.20$  region is clean but whose  $\lambda 1550.77$  region contains bad pixels, and “3” for systems that contain bad pixels in both the  $\lambda\lambda 1548.20, 1550.77$  regions. In the above, “ $\lambda 1548.20$  region” refers to the spectral region within  $\pm 30 \text{ km s}^{-1}$  of the expected C IV  $\lambda 1548.20$  line center; likewise for  $\lambda 1550.77$ .

We then formed composite spectra by shifting the spectrum of each system with certain chosen flag(s) (see section 3.3) to the rest frame of the Ly $\alpha$  line, rebinning the rest-frame spectrum onto a common velocity scale of bin size of  $3.3 \text{ km s}^{-1}$  (half the nominal resolution of the HIRES spectra), and averaging all the rest-frame spectra in the C IV region weighted by the square of S/N at each bin. We also tried weighting each spectrum by the square of the mean S/N within  $\pm 30 \text{ km s}^{-1}$  of the C IV  $\lambda 1548$  line, with negligible change in the results.

To estimate the equivalent width of the C IV absorption in a composite spectrum, a continuum was first fitted to the composite spectrum using cubic splines after excluding the  $\pm 30 \text{ km s}^{-1}$  region centered on the  $\lambda 1548.20$  position. We then measured the equivalent width of C IV  $\lambda 1548.20$  by directly integrating over the  $\pm 25 \text{ km s}^{-1}$  region centered on the position of C IV  $\lambda 1548.20$ , where  $\pm 25 \text{ km s}^{-1}$  corresponds to 3 times the (assumed) FWHM of the C IV absorption for  $b = 10 \text{ km s}^{-1}$  based on profile fitting to C IV absorption systems detected in other HIRES spectra (cf. Rauch et al 1996). We had to assume a  $b$  value for the C IV absorption since no actual detection was made in any of the composite spectra (section 3.3).

Because no C IV absorption was detected in the composite spectra, we estimated the equivalent width limit from Monte Carlo simulations. For each quasar spectrum, we first picked redshifts randomly within the redshift range over which the actual Ly $\alpha$  lines that were used to form a composite spectrum were found. The number of redshifts picked was the same as the observed number of Ly $\alpha$  lines. We then treated these random redshifts as positions of Ly $\alpha$  lines, assigned a flag to each redshift according to the “cleanness” of the C IV region. We then formed a composite spectrum using these random redshifts and measured the equivalent width at the line position of C IV  $\lambda 1548.20$  in exactly the same way as was done for the real data. This procedure was repeated 4000 times. The resulting distribution of measured equivalent width at the position of C IV  $\lambda 1548.20$  was then examined to infer the 95.5% confidence limit on the equivalent width of C IV  $\lambda 1548.20$  absorption in the composite spectrum, which corresponds to a  $2\sigma$  upper limit if the distribution is Gaussian. The actual distributions of the measurement equivalent widths from the simulations closely resemble a Gaussian function.

### 3.2. Abundance Estimates

The 95.5% confidence limit obtained above for each sample combined with the expected mean  $N(\text{H I})$  of the sample (column 5 of Table 4) yields a  $N(\text{C IV})/N(\text{H I})$  upper limit for the sample. In order to turn the  $N(\text{C IV})/N(\text{H I})$  limit into an estimate of the C abundance in the clouds, one must know the ionization conditions in the gas. Since only  $N(\text{H I})$  is known, it is not possible to constrain the ionization conditions from the ionic ratios.

Recent hydrodynamical simulations of cosmological structure formation in the context of the Cold Dark Matter or other models have been generally successful in matching the observed characteristics of Ly $\alpha$  forest clouds over the redshift range  $2 < z < 4$  (Cen et al 1994; Petitjean,



Mucket, & Kates 1995; Zhang, Anninos, & Norman 1995; Hernquist et al 1995; Miralda-Escude et al 1996; Rauch et al 1997). In these models, the higher  $N(\text{H I})$  clouds ( $N(\text{H I}) > 10^{14} \text{ cm}^{-2}$  or so) tend to be associated with filaments surrounding and connecting collapsed objects, while the lower  $N(\text{H I})$  clouds tend to be found in voids. Rauch et al (1997) addressed the ionization state of the  $\text{Ly}\alpha$  clouds and heavy elements and showed that the observed  $N(\text{C IV})/N(\text{H I})$  vs  $N(\text{H I})$  follows the predicted relation from the simulations if a mean  $[\text{C}/\text{H}] = -2.5$  is assumed for the gas. Given the lack of observational constraints on the ionization conditions in the  $\text{Ly}\alpha$  clouds in our sample and considering the reasonable success of the simulations, it seems appropriate to use their theoretical prediction of  $N(\text{C IV})/N(\text{H I})$  vs  $N(\text{H I})$  to estimate  $[\text{C}/\text{H}]$  for our  $\text{Ly}\alpha$  clouds. An added benefit of using this relation is that the metallicity of the lower column density clouds considered here and that of the higher column density ( $N(\text{H I}) > 10^{14.5} \text{ cm}^{-2}$ ) clouds considered by Rauch et al are derived in a self-consistent manner.

The  $N(\text{C IV})/N(\text{H I})$  vs  $N(\text{H I})$  relation of Rauch et al (1997) over  $10^{13.5} < N(\text{H I}) < 10^{14} \text{ cm}^{-2}$  can be described by the function

$$\log N(\text{CIV})/N(\text{HI}) = 0.90 \times \log N(\text{HI}) - 14.80 \quad (1)$$

for  $[\text{C}/\text{H}] = -2.5$ . This relation was used to infer  $[\text{C}/\text{H}]$  for the various composite spectra discussed in section 3.3. The conversion from  $N(\text{C IV})/N(\text{H I})$  to  $[\text{C}/\text{H}]$  was probably the most uncertain step in the entire analysis. Unfortunately, it was not possible to estimate the magnitude of this uncertainty. However, because the same  $N(\text{C IV})/N(\text{H I})$  vs  $N(\text{H I})$  relation (i.e., equation (1)) was used to derive metallicities for both the  $10^{13.5} < N(\text{H I}) < 10^{14} \text{ cm}^{-2}$  clouds (this study) and the  $N(\text{H I}) > 10^{14.5} \text{ cm}^{-2}$  clouds (Rauch et al), the relative metallicities between these clouds should be reasonably accurate.

### 3.3. Results

The results from analyzing the composite spectra for several samples (next paragraph) are tabulated in Table 4. Column 1 of Table 4 gives a letter identifying each sample. The second and third columns give the total number of lines in the sample and the mean redshift of the lines in the sample. Column 4 indicates the estimated S/N per  $6.6 \text{ km s}^{-1}$  resolution element in the composite spectrum based on propagation of the individual error spectra. Column 5 is the expected mean  $N(\text{H I})$  of the sample from the  $f(N) \propto N^{-1.5}$  distribution. Column 6 gives the upper limit of the rest frame equivalent width of  $\text{C IV } \lambda 1548.20$  from the composite spectrum at the 95.5% confidence level based on the Monte Carlo simulations discussed in section 3.1. Column 7 gives the 95.5% confidence limit on  $N(\text{C IV})$  derived from the equivalent width limits in column 6 assuming that such weak lines are on the linear part of the curve of growth. The last column gives the metallicity limit at the 95.5% confidence level based on the  $N(\text{C IV})/N(\text{H I})$  limit as described in section 3.2.

Following convention, we treat the clouds within  $3,000 \text{ km s}^{-1}$  of the emission redshift of the

background quasars separately from those further away from the emission redshift of the quasars for several reasons: (1) clouds very close to the quasar emission redshifts may be physically close to the background quasars and may be more highly ionized due to the enhanced UV ionizing flux. (2) the heavy element absorption systems within  $3,000 \text{ km s}^{-1}$  of  $z_{em}$  often show N v and relatively high metallicities, suggesting that many of them may be ejected from the background quasars or related to their host galaxies or their immediate environments.

We first formed a composite spectrum using 233 Ly $\alpha$  lines in Table 2 that are more than  $3,000 \text{ km s}^{-1}$  away from  $z_{em}$  and that have flag=0; the latter ensures that both the C iv  $\lambda 1548.20$  and  $\lambda 1550.77$  line regions in the composite spectrum contain contributions from the same Ly $\alpha$  systems. No significant C iv absorption was seen in the composite spectrum. In order to maximize the S/N of the composite spectra in the C iv  $\lambda 1548.20$  region, we decided to also include Ly $\alpha$  lines with flag=2 in the analysis.

We considered the following 7 samples:

*Sample A:* All Ly $\alpha$  lines in Table 2 with flag=0 or 2 that are more than  $3,000 \text{ km s}^{-1}$  away from  $z_{em}$ .

*Sample B:* All Ly $\alpha$  lines in Table 2 with flag=0 or 2 that are more than  $3,000 \text{ km s}^{-1}$  away from  $z_{em}$  and that have estimated  $N(\text{H I}) < 13.75$  (i.e.,  $10^{13.5} < N(\text{H I}) < 10^{13.75} \text{ cm}^{-2}$ ) based on the residual flux at the line center assuming Doppler  $b = 25 \text{ km s}^{-1}$ .

*Sample C:* All Ly $\alpha$  lines in Table 2 with flag=0 or 2 that are more than  $3,000 \text{ km s}^{-1}$  away from  $z_{em}$  and that have estimated  $N(\text{H I}) > 13.75$  (i.e.,  $10^{13.75} < N(\text{H I}) < 10^{14} \text{ cm}^{-2}$ ) based on the residual flux at the line center assuming  $b = 25 \text{ km s}^{-1}$ .

*Sample D:* All Ly $\alpha$  lines in Table 2 with flag=0 or 2 that are more than  $3,000 \text{ km s}^{-1}$  away from  $z_{em}$  and that have  $z < 2.75$ .

*Sample E:* All Ly $\alpha$  lines in Table 2 with flag=0 or 2 that are more than  $3,000 \text{ km s}^{-1}$  away from  $z_{em}$  and that have  $z > 2.75$ .

*Sample F:* All Ly $\alpha$  lines in Table 2 with flag=0 or 2 that are more than  $3,000 \text{ km s}^{-1}$  away from  $z_{em}$  and that are within  $200 \text{ km s}^{-1}$  of known metal systems.

*Sample G:* All Ly $\alpha$  lines in Table 2 with flag=0 or 2 that are within  $3000 \text{ km s}^{-1}$  of  $z_{em}$ . There are only 12 lines in this sample.

None of the composite spectra showed significant C iv absorption. The composite spectrum for sample A, which is the average of 282 Ly $\alpha$  lines and which has an estimated S/N of 1860:1 per  $6.6 \text{ km s}^{-1}$  (the resolution of the original HIRES spectra), is shown in Figure 3 as an example. This S/N is  $\sim 10$  times better than the best S/N in the C iv region of individual spectra, and is  $\sim 20$  times better than the *average* S/N of the spectra. The composite spectrum has a mean flux extremely close to unity (as expected) but with some mild undulation, probably as a result of imperfect continuum placement in the original spectra.

## 4. DISCUSSION

### 4.1. Implications of the Lack of Detection of Metals in the Low Column Density Clouds

The results tabulated in Table 4 can be summarized briefly as the follows:

(1) Excluding the few Ly $\alpha$  clouds that show C IV absorption individually, Ly $\alpha$  clouds with  $10^{13.5} < N(\text{H I}) < 10^{14} \text{ cm}^{-2}$  and  $2.2 < z < 3.6$  have *mean* [C/H] < -3.5 at the 95.5% confidence level. This upper limit is a factor of 10 smaller than the mean [C/H] found for similar Ly $\alpha$  clouds with  $N(\text{H I}) > 10^{14.5} \text{ cm}^{-2}$  (Cowie et al 1995; Tytler et al 1995; Songaila & Cowie 1996; Rauch et al 1997; Hellsten et al 1997). The above conclusion appears to hold, to within a factor of  $\sim 2$ , independent of redshift or  $N(\text{H I})$  for the ranges considered above.

(2) Again, excluding the few clouds that show C IV absorption individually, Ly $\alpha$  clouds with  $10^{13.5} < N(\text{H I}) < 10^{14} \text{ cm}^{-2}$  and  $2.2 < z < 3.6$  have *mean* [C/H] < -3.0 at the 95.5% confidence level even when they are within  $200 \text{ km s}^{-1}$  of known metal systems.

(3) Once again, excluding the few clouds that show C IV absorption individually, Ly $\alpha$  clouds with  $10^{13.5} < N(\text{H I}) < 10^{14} \text{ cm}^{-2}$  and  $2.2 < z < 3.6$  have *mean* [C/H] < -2.7 at the 95.5% confidence level even when they are within  $3000 \text{ km s}^{-1}$  of the emission redshift of the background quasars. This upper limit is a factor of  $> 7 - 500$  lower than for similar clouds that show C IV absorption individually (see “associated” systems in Table 3 and section 4.2). It is quite possible that these clouds occur within  $3000 \text{ km s}^{-1}$  of the emission redshift of the background quasars solely by accident and that they are not related in anyway to the background quasars. In other words, they belong to the class of “intervening” clouds despite their proximity in redshift to the background quasars.

The mean metallicity of the Ly $\alpha$  clouds with  $10^{13.5} < N(\text{H I}) < 10^{14} \text{ cm}^{-2}$ , [C/H] < -3.5, is in stark contrast to that of the Ly $\alpha$  clouds with  $N(\text{H I}) > 10^{14.5} \text{ cm}^{-2}$  for which several studies have found that 50-75% of these clouds show detectable C IV absorption in individual HIRES spectra with a mean [C/H]  $\simeq -2.5$  (Cowie et al 1995; Tytler et al 1995; Songaila & Cowie 1996; Rauch et al 1997; Hellsten et al 1997). Surprisingly, the Ly $\alpha$  clouds with  $10^{13.75} < N(\text{H I}) < 10^{14} \text{ cm}^{-2}$ , with a mean  $N(\text{H I})$  that is only a factor of  $\sim 4$  smaller than the limiting  $N(\text{H I}) = 10^{14.5} \text{ cm}^{-2}$  probed by previous studies, are found to have a mean [C/H] < -3.55 or a factor of 11 lower. These results suggest that a rapid decrease with decreasing  $N(\text{H I})$  in the mean metallicity level of the clouds sets in at  $N(\text{H I}) \sim 10^{14} - 10^{14.5} \text{ cm}^{-2}$ .

In figure 4 we show very crudely the metallicity distribution of quasar absorption line systems as a function of  $N(\text{H I})$ . The effects of non-solar relative abundances are ignored. A trend of decreasing metallicity with decreasing  $N(\text{H I})$  is indicated by figure 4. Since the higher column density systems are likely to be more intimately associated with collapsed objects, where star formation is expected to occur earlier and more vigorously, the above trend of decreasing

metallicity with decreasing  $N(\text{H I})$  is consistent with the scenario in which star formation in collapsed objects eject metal-enriched material outwards and pollute their surroundings.

The detection of C IV absorption in individual Ly $\alpha$  clouds with  $N(\text{H I})$  as low as  $10^{14.5}$   $\text{cm}^{-2}$  in high sensitivity Keck observations was considered evidence for the occurrence of an early generation of stars (Pop III) that may have polluted the entire universe in a wide spread fashion to a nearly uniform level of  $[\text{C}/\text{H}] \simeq -2.5$  (Songaila & Cowie 1996). A similar inference was made by Lu, Sargent, & Barlow (1997) based on the rough agreement between the metallicity,  $[\text{C}/\text{H}] \simeq -2.5$ , that was inferred for the Ly $\alpha$  clouds and that of the lowest metallicity damped Ly $\alpha$  galaxies, generally believed to be the high-redshift progenitors of normal galaxies (Wolfe 1988). However, the extremely low metallicities we infer for the Ly $\alpha$  clouds with  $10^{13.5} < N(\text{H I}) < 10^{14}$   $\text{cm}^{-2}$  rule out the scenario of uniform contamination by Pop III stars to  $[\text{C}/\text{H}] \sim -2.5$ . Recent theoretical studies appear to corroborate this results. For example, Ostriker & Gnedin (1996) and Gnedin & Ostriker (1997; see also Murakami & Yamashita 1997; Steinmetz 1997) recently explored the process of early metal enrichment using high resolution numerical simulations. In the COBE-normalized Cold Dark Matter plus cosmological constant model investigated by these authors, the first generation of stars (Pop III) occurred at a redshift of  $z \sim 14$  through molecular hydrogen cooling. Subsequent supernova explosions from such stars then enriched the universe to a mean metallicity of  $10^{-3.7}$  solar, which is considerably lower than the mean  $[\text{C}/\text{H}] \simeq -2.5$  found for Ly $\alpha$  clouds with  $N(\text{H I}) > 10^{14.5}$   $\text{cm}^{-2}$  but is consistent with the upper limit found for Ly $\alpha$  clouds with  $10^{13.5} < N(\text{H I}) < 10^{14}$   $\text{cm}^{-2}$ . The energy release from the supernova also raised the temperature of the gas and destroyed the hydrogen molecules through photodissociation, thus temporarily shutting down the star formation process. It was not until  $z < 10$  when hydrogen line cooling became sufficient to induce a second major episode of star formation (Pop II). Interestingly, Gnedin & Ostriker predicted that there should be a sharp drop in the metallicity level of Ly $\alpha$  clouds at column density below about  $10^{13.5} - 10^{14.5}$   $\text{cm}^{-2}$  at  $z = 4$  (see their figure 7), a feature apparently confirmed by our result.

In view of all the evidence, we conclude that, if a generation of Pop III stars occurred in the very early universe, the mean enrichment level of the intergalactic medium resulting from the associated supernova should be  $[\text{C}/\text{H}] < 10^{-3.5}$ . The relatively high metallicities,  $[\text{C}/\text{H}] \simeq -2.5$ , found for the  $N(\text{H I}) > 10^{14.5}$   $\text{cm}^{-2}$  clouds are best explained by later enrichment from Pop II stars occurring either within the clouds themselves or in nearby galaxies.

It is possible to obtain some clues about the size scale of the metal-enriched (i.e.,  $[\text{C}/\text{H}] \simeq -2.5$ ) regions. If we assume that the observed velocity spread  $\Delta v$  of the components in C IV systems are purely due to ejection of metal-enriched gas from supernova, we can set a conservative upper limit on the maximum distance this enriched gas could have traveled by the time of observations. This distance is of the order of 200 kpc if a typical  $\Delta v = 400$   $\text{km s}^{-1}$  is adopted and if it is assumed that the first supernova occurred  $\sim 1$  Gyrs before our observation ( $z \sim 3$ ). The lack of detectable metals in Ly $\alpha$  clouds within 200  $\text{km s}^{-1}$  of known metal systems puts another limit on the spatial size of the enriched region to be  $< 500 h_{50}^{-1}$  kpcs if it is assumed that this velocity difference is

purely due to Hubble flow. Finally, according to simulations, the  $N(\text{H I}) = 10^{14} \text{ cm}^{-2}$  contour, which roughly separates metal-rich gas with  $[\text{C}/\text{H}] \simeq -2.5$  from metal-poor gas with  $[\text{C}/\text{H}] < -3.5$ , delineates a continuous filamentary gaseous structure in which galaxies are embedded. The thickness of this structure is of the order 100 kpcs (Rauch et al 1997), in broad agreement with other estimates.

#### 4.2. Metallicity and Nature of Low $N(\text{HI})$ $\text{Ly}\alpha$ Systems with Detectable C IV Absorption

As noted briefly in section 2.2, some of the low column density  $\text{Ly}\alpha$  clouds considered here show detectable C IV absorption individually (figure 2 and Table 3). This is in stark contrast with the vast majority of systems with similar  $N(\text{H I})$  whose composite spectra did not reveal any C IV absorption down to very sensitive limits (Table 4).

To understand the nature of these low  $N(\text{H I})$   $\text{Ly}\alpha$  clouds that apparently contain a significant amount of metals, we estimated the lower limit to their metallicity adopting the usual assumption that the clouds are photoionized by the integrated light from quasars. We ran several set of photoionization models using CLOUDY v90.02 (Ferland 1996) assuming plane-parallel geometry and uniform gas density for the clouds. We considered several plausible ionizing spectra: (1) the mean quasar spectrum constructed by Haardt & Madau (1996; hereafter HM) assuming a transparent universe; the spectrum has a spectral index  $\alpha = -1.5$  over the critical 1-4 Rydberg region; (2) the above spectrum after taking into account the opacity of intervening clouds as calculated by HM (their spectrum at redshift  $z = 3$  is adopted); Two further ionizing spectra considered were similar to the two mentioned above but with  $\alpha = -1.8$  over 1-4 Rydberg region. These latter spectra, which were also from HM (private communication), were calculated in light of the work by Zheng et al (1998) and Laor et al (1997) after the HM paper had appeared in press. The CLOUDY results gave predictions about the variation of  $N(\text{C IV})$  as a function of the ionization parameter,  $\Gamma$  (the ratio of ionizing photon density to hydrogen gas particle density) for chosen  $N(\text{H I})$  and metallicity. For a given system with measured  $N(\text{H I})$  and  $N(\text{C IV})$ , we estimated a lower limit to  $[\text{C}/\text{H}]$  by assuming that the C IV/H I ratio is at the peak of the distribution. This approach resulted in the  $[\text{C}/\text{H}]$  lower limits given in column 7 ( $[\text{C}/\text{H}]_{\text{P}}$ ) of Table 3, where the CLOUDY results based on the  $\alpha = -1.8$  HM spectrum without intervening opacity was used for the “associated” systems, and the CLOUDY results based on the  $\alpha = -1.8$  HM spectrum taking into account the intervening opacity was used for the “intervening” systems. The ratio of C IV/H I typically peaks at  $\Gamma = -1 \pm 0.5$  in these models. The  $[\text{C}/\text{H}]$  lower limits were  $\sim 0.4$  dex higher than these given in Table 3 for the “intervening” systems if the  $\alpha = -1.5$  HM spectrum with intervening opacity was adopted. Similarly, the  $[\text{C}/\text{H}]$  lower limits would be  $\sim 0.2$  dex higher for the “associated” systems if the  $\alpha = -1.5$  HM spectrum without intervening opacity was adopted. Accordingly, the  $[\text{C}/\text{H}]_{\text{P}}$  limits given in Table 3 are relatively conservative

estimates.<sup>6</sup>

It is possible that the clouds given in Table 3 are collisionally ionized rather than photoionized. Earlier studies (Blades 1988, and references therein; Rauch et al 1996) found that the line widths of many C IV absorption lines are too narrow to be collisionally ionized. However, the conditions in the very low column density clouds considered here could be different. For gas that is in collisional ionization equilibrium, the ratio of C IV/H I peaks at temperature  $T = 10^{5.05}$  K with  $C\text{ IV}/H\text{ I} = 10^{4.3} C/H$  (Sutherland & Dopita 1993). For solar metallicity, this implies  $C\text{ IV}/H\text{ I} = 7.2$ . In comparison, the peak C IV/H I value is around unity for the photoionization models considered above when solar metallicity is assumed. Thus collisionally ionized clouds could reach much higher C IV/H I ratio than photoionized clouds for the same metallicity. The  $[C/H]$  limits derived from collisional ionization assuming the peak C IV/H I ratio are given in column 8 ( $[C/H]_C$ ) of Table 3. However, the widths of all but one of the Ly $\alpha$  absorption lines imply  $T < 10^{4.7}$  K, which is inconsistent with these clouds being collisionally ionized at  $T \sim 10^5$  K. It could be argued that the observed Ly $\alpha$  absorption is not responsible for the C IV absorption. In this case, the Ly $\alpha$  absorption corresponding to the collisionally-ionized C IV absorption could be broad ( $b = 41$  km s<sup>-1</sup> for  $T = 10^5$  K) and shallow and may be hidden for some of the systems. However, 3 of the 7 intervening systems in Table 3 have temperature  $T < 10^{4.6}$  K based on the width of the C IV absorption lines. Similarly, 2 of 8 of the associated systems in Table 3 have  $T < 10^{4.6}$  K based on the width of the C IV absorption. Clearly the C IV in these clouds cannot be produced by collisional ionization at  $T \sim 10^5$  K under equilibrium conditions. It is perhaps no coincidence that almost all the C IV absorption lines with inferred  $T < 10^5$  K are relatively strong and well measured, while those with inferred  $T > 10^5$  K are all relatively weak, suggesting that the temperature of the latter systems may have been overestimated owing to our inability to discern the component structure. We therefore conclude these clouds are not likely to be collisionally ionized under equilibrium conditions.

However, the clouds which show detectable C IV absorption could be collisionally ionized under non-equilibrium conditions. Indeed, hot plasma gas cools very fast over the  $T \sim 10^5$  K regime. As shown in figure 15 of Sutherland & Dopita (1993), the cooling time for gas with solar composition at  $T \sim 10^5$  K is shorter than the time to reach collisional ionization equilibrium for C IV and especially for C V. Consequently, the overall ionization balance of C is governed by the slowly recombining C V ion. Figure 16 of Sutherland & Dopita indicates that large fractions of C IV, C V, and C VI ions can exist at temperature as low as  $10^{4.5}$  K under non-equilibrium conditions, while under collisional ionization equilibrium the fractions of these ions at such a low temperature would be negligible. These considerations raise the possibility that the C IV ions

---

<sup>6</sup>Incidentally, if we use the relation between  $\log N(C\text{ IV})/N(H\text{ I})$  and  $\log N(H\text{ I})$  from Rauch et al (1997; equation (1) of this paper) to estimate the actual metallicity of the intervening systems, as was done for the composite spectra, the resulting  $[C/H]_P$  values (no longer lower limits) will be 0.05 to 0.35 dex higher than the lower limits quoted in Table 3 for these systems. The relative small differences suggest that the clouds in the Rauch et al simulations are near the peak of C IV/H I distribution.

in the Ly $\alpha$  clouds listed in Table 3 with  $T < 10^{4.6}$  K could be produced by collisional ionization but under non-equilibrium conditions. However, figure 16 of Sutherland & Dopita also indicates that  $N(\text{C II}) > N(\text{C IV})$  under such conditions. When the likely sub-solar metallicities of the Ly $\alpha$  clouds are taken into account, we infer from figures 9, 14, and 15 of Sutherland & Dopita that the actual cooling time scale in the clouds is likely to be shorter than the collisional ionization equilibrium time scale of C II and C V but longer than that of C IV. This should further *increase*  $N(\text{C II})$  relative to  $N(\text{C IV})$  because more C IV should recombine to C III than can be created through the recombination of C V. As a result, we expect to detect C II  $\lambda 1334$  absorption in these Ly $\alpha$  systems if the C IV ions were produced by collisional ionization at  $T < 10^{4.6}$  K under non-equilibrium conditions. No C II  $\lambda 1334$  absorption is found in any of the systems listed in Table 3 in our HIRES spectra (the C II  $\lambda 1334$  regions for three of the systems are contaminated by unrelated absorption lines).

It therefore seems likely that the clouds showing detectable C IV absorption are photoionized rather than collisionally ionized. Assuming this is the case, one then find that the intervening clouds have metallicities ranging from  $[\text{C}/\text{H}] > -2.2$  to  $[\text{C}/\text{H}] > -0.9$  (see column 7 of Table 3), which is significantly higher than for typical Ly $\alpha$  clouds of similar  $N(\text{H I})$ . Several of the associated systems have  $[\text{C}/\text{H}]$  within a factor of 2 of the solar metallicity. This result is consistent with previous work (Savaglio, D’Odorico, & Moller 1994; Petitjean, Rauch, & Carswell 1994; Tripp, Lu, & Savage 1996) and it indicates rapid enrichment in the quasar nuclei/environment. The same characteristics appear to be shared by the broad absorption line clouds and broad emission line clouds (cf. Hamann 1997, and references therein). A few of the what we classify as “associated” systems (because they are within  $3,000 \text{ km s}^{-1}$  of  $z_{em}$ ) actually have  $[\text{C}/\text{H}]$  lower limits comparable to most of the intervening systems; some of these could be clouds that are unrelated to the quasar environment but happen to have redshifts close to  $z_{em}$ .

The inferred lower limits of  $[\text{C}/\text{H}]$  for the intervening clouds listed in Table 3 are factors 20-400 (or more) higher than the mean  $[\text{C}/\text{H}] < -3.5$  found for the vast majority of intervening clouds (Table 4). What are the causes of such large differences? We consider two possibilities: (1) the intervening clouds which show individual C IV absorption could represent the high metallicity tail of the metallicity distribution of the Ly $\alpha$  clouds; (2) the intervening clouds with detectable C IV absorption have a separate origin: perhaps they are ejected from the background quasar despite the large ejection velocities ( $> 10,000 \text{ km s}^{-1}$ ) required, or they may be ejected from foreground quasars near the quasar sight line, in which case extremely large ejection velocity are no longer required. The latter possibility of case (2) above could be check by searching for foreground quasars near the redshifts of the Ly $\alpha$  systems that show detectable C IV absorption. However, that the “intervening” systems listed in Table 3 seem to have lower C IV/H I ratios on average than the “associated” systems suggests that they are probably not ejected from quasars.

We now consider in some detail the more interesting case (1) above. If the weak Ly $\alpha$  lines in our sample have a broad distribution in metallicity and if the intervening clouds showing C IV absorption indeed represent the high metallicity tail of that distribution, two conditions

should be met. Take sample A for example. First, the metallicity distribution in the clouds must be such that 6<sup>7</sup> of 282+6 randomly-drawn systems should have  $[C/H] > -2.17$ . Second, the composite spectrum of the remaining 282 systems must not show C IV  $\lambda 1548$  absorption with  $w_r(1548) > 0.088$  mÅ or  $N(C\text{ IV}) > 10^{10.34}$  cm<sup>-2</sup> (Table 4).

In order to examine the above conditions quantitatively, we explore the following simple model. We assume that the  $[C/H]$  distribution of the clouds can be described by a Gaussian function with a mean metallicity  $M_0$  and a standard dispersion  $\sigma_M$ . The first condition, that 6 of 288 randomly-drawn systems have  $[C/H] > -2.17$  then requires that  $[C/H] = -2.17$  is  $2.04\sigma_M$  away from  $M_0$ . In other words:

$$-2.17 - M_0 = 2.04\sigma_M \quad (2).$$

For the second condition, it can be shown that, for an ensemble of clouds drawn randomly from the H I column density distribution  $f(N) \propto N^{-1.5}$  and the above metallicity distribution, the mean column density of C IV is

$$N(C\text{ IV}) = \sum N(H\text{ I})^{1.9} \times 10^{[C/H]-12.30}/N_l, \quad (3)$$

where  $N_l$  is the total number of lines in the sample. Here, equation (1) has been used to derive  $N(C\text{ IV})$  for individual cloud from the  $N(H\text{ I})$  and  $[C/H]$  values drawn from the distributions. The sum in equation (3) can be estimated numerically. Strictly speaking, one should take into account the variable detection sensitivity (i.e., variable S/N) of the spectra in the above analysis. However, given the crudeness of this analysis, and considering the relative uniformity of the HIRES spectra, assuming a uniform detection sensitivity for this analysis probably suffice for our purposes.

Equation (2) maps out a straight line in the  $M_0$  vs  $\sigma_M$  plane, while equation (3) combined with the requirement  $N(C\text{ IV}) < 10^{10.34}$  cm<sup>-2</sup> maps out a region in the  $M_0$  vs  $\sigma_M$  plane. The results are shown in Figure 5, where the solid straight line is equation (2). The shaded area indicates the  $[M_0, \sigma_M]$  combinations for which the composite spectrum of 282 randomly drawn Ly $\alpha$  systems, subject to the condition  $[C/H] < -2.17$ , would not reveal a C IV  $\lambda 1548.20$  absorption with mean  $N(H\text{ I}) > 10^{10.34}$  cm<sup>-2</sup> at the 90% confidence level. The solid line connecting the dots gives the  $[M_0, \sigma_M]$  relation for which the composite spectrum of 282 randomly drawn Ly $\alpha$  systems (again, subject to the condition  $[C/H] < -2.17$ ) would produce a C IV  $\lambda 1548.20$  absorption with a mean  $N(C\text{ IV}) = 10^{10.34}$  cm<sup>-2</sup>. It is seen that only at  $\sigma_M > 1$  or so is there any overlap between the straight line and the shaded area, when the two conditions mentioned above are met simultaneously. Thus, within the validity of the simple model explored here, if the 7 intervening Ly $\alpha$  systems with  $10^{13.5} < N(H\text{ I}) < 10^{14}$  cm<sup>-2</sup> that individually show C IV absorption are drawn from the same population as the remaining Ly $\alpha$  systems with similar  $N(H\text{ I})$  which do not show detectable C IV absorption, then the overall metallicity distribution of the clouds must be such that it has a mean metallicity  $[C/H] < -4$  with a dispersion  $> 1$  dex. This is roughly consistent

---

<sup>7</sup>One of the intervening systems listed in Table 3 ( $z = 3.13247$  toward Q1422+2309) is within 50 km s<sup>-1</sup> of a strong Ly $\alpha$  line and does not qualify to be included in our sample.



with the mean metallicity of  $10^{-3.7}$  predicted by Ostriker & Gnedin (1996) for the enrichment by Pop III stars.

## 5. SUMMARY AND CONCLUSIONS

We have investigated the metal contents of Ly $\alpha$  clouds at  $2.2 < z < 3.6$  with  $10^{13.5} < N(\text{H I}) < 10^{14} \text{ cm}^{-2}$  using high resolution (FWHM=6.6 km s $^{-1}$ ), high S/N ( $\sim 100:1$ ) spectra obtained with the 10m Keck I telescope. Previous investigations of similar nature were limited to Ly $\alpha$  clouds with  $N(\text{H I}) > 10^{14.5} \text{ cm}^{-2}$  for which a mean metallicity of  $[\text{C}/\text{H}] \simeq -2.5$  was deduced. It has been suggested that the metals seen in these clouds may have been produced by a generation of Population III stars occurred at a much earlier epoch before the formation of quasars and normal galaxies. From 9 of our best S/N quasar spectra obtained with the HIRES, we selected  $\sim 300$  Ly $\alpha$  lines with estimated  $N(\text{H I})$  between  $10^{13.5} < N(\text{H I}) < 10^{14} \text{ cm}^{-2}$ . The Ly $\alpha$  lines selected have absorption redshift  $2.2 < z_{\text{abs}} < 3.6$  (excluding Ly $\alpha$  lines within 3000 km s $^{-1}$  of the quasar emission redshifts). After eliminating a small number of Ly $\alpha$  lines that individually show detectable C IV absorption (see point 4 below), we shifted the quasar spectra into the rest frame of each of the remaining Ly $\alpha$  clouds in the sample and then averaged the rest-frame spectra over the spectral region encompassing the C IV  $\lambda\lambda 1548.20, 1550.77$  absorption lines. We reached S/N as high as 1860:1 per 6.6 km s $^{-1}$  resolution element in our composite spectra. Such a high S/N would have been impossible to obtain through direct observations. The main conclusions are as follows:

(1) No significant C IV absorption was detected in any of the composite spectra we investigated. The most sensitive limit was obtained when all Ly $\alpha$  lines in the sample (excluding those showing C IV absorption individually) that are more than 3,000 km s $^{-1}$  away from the background quasars were included in the analysis, for which we reached a S/N=1860:1 per resolution element, corresponding to an upper limit of  $< 0.088 \text{ m}\text{\AA}$  (95.5% confidence limit) for the rest-frame equivalent width of the C IV  $\lambda 1548.20$  line. We deduced a mean metallicity of  $[\text{C}/\text{H}] < -3.5$  for these clouds using the cosmological simulations of Rauch et al (1997) to infer the ionization correction; the same simulation results have been used previously to deduce a mean metallicity of  $[\text{C}/\text{H}] \simeq -2.5$  for Ly $\alpha$  clouds with  $N(\text{H I}) > 10^{14.5} \text{ cm}^{-2}$ . The low metallicities derived for the  $10^{13.5} < N(\text{H I}) < 10^{14} \text{ cm}^{-2}$  clouds appear to hold to within a factor of  $\sim 2$  independent of redshift or  $N(\text{H I})$  over the range considered above. In particular, a sample of Ly $\alpha$  clouds occurring within 200 km s $^{-1}$  of known metal systems yielded a mean metallicity of  $[\text{C}/\text{H}] < -3.0$  (95.5% confidence limit) based on a composite spectrum analysis.

(2) The mean metallicity of Ly $\alpha$  clouds with  $10^{13.5} < N(\text{H I}) < 10^{14} \text{ cm}^{-2}$ ,  $[\text{C}/\text{H}] < -3.5$ , is a factor of 10 lower than that inferred for Ly $\alpha$  clouds with  $N(\text{H I}) > 10^{14.5} \text{ cm}^{-2}$ . This suggests that a sharp drop in the metallicity level of Ly $\alpha$  clouds sets in at  $N(\text{H I}) = 10^{14} - 10^{14.5} \text{ cm}^{-2}$ . This result rules out the suggestion that a generation of Pop III stars could have polluted the entire universe to a uniform level of  $[\text{C}/\text{H}] \simeq -2.5$ . Cosmological simulations involving gas hydrodynamics

indicate that Ly $\alpha$  absorption with  $N(\text{H I}) > 10^{14.5} \text{ cm}^{-2}$  mostly occurs in continuous filaments of gas surrounding and connecting collapsed objects, while those with  $N(\text{H I}) < 10^{14} \text{ cm}^{-2}$  are preferentially found in void regions further away from collapsed objects. These results, coupled with theoretical predictions about Pop III star formation and enrichment (Ostriker & Gnedin 1996; Gnedin & Ostriker 1997), strongly suggest that most of the heavy elements in Ly $\alpha$  clouds with  $N(\text{H I}) > 10^{14.5} \text{ cm}^{-2}$  were probably produced *in situ* by Pop II stars, in the sense that they were either made by stars within the clouds or were ejected from nearby star-forming galaxies. Consequently, the void regions ( $N(\text{H I}) < 10^{14} \text{ cm}^{-2}$ ) could only have experienced the enrichment by Pop III stars. We estimated a typical thickness of the order of 100 kpc at  $z = 3$  for the metal-enriched filamentary structures.

(3) The low metallicities we inferred for the Ly $\alpha$  clouds with  $10^{13.5} < N(\text{H I}) < 10^{14} \text{ cm}^{-2}$  require that, if there was a generation of Pop III stars that occurred in the very early universe, the mean enrichment level resulting from the explosions of such stars should be  $[\text{C}/\text{H}] < -3.5$  for Ly $\alpha$  clouds with  $10^{13.5} < N(\text{H I}) < 10^{14} \text{ cm}^{-2}$  at  $2.2 < z < 3.6$ , or  $[\text{C}/\text{H}] < -4$  if the Ly $\alpha$  clouds which individually show detectable C IV absorption are to be considered part of the overall metallicity distribution (point 4 below). These results are consistent with the recent theoretical calculations of Ostriker & Gnedin (1996).

(4) A small fraction (16) of the Ly $\alpha$  clouds with  $10^{13.5} < N(\text{H I}) < 10^{14} \text{ cm}^{-2}$  show detectable C IV absorption individually (figure 2 and Table 3). Of the 16 systems, 9 occur within  $3,000 \text{ km s}^{-1}$  of the emission redshift of the background quasars and may be gas ejected from the quasars or gas associated with the quasar host galaxies and/or their environment. Most of these clouds are inferred to have  $[\text{C}/\text{H}]$  close to or even exceeding the solar value based on photoionization models, consistent with previous studies. The remaining 7 systems have velocities  $> 10,000 \text{ km s}^{-1}$  away from the emission redshift of the background quasars and are likely to be intervening in nature. Collisional ionization is ruled out for at least 3 of the 7 intervening clouds based on the width of the C IV absorption lines. If the clouds are photoionized by the integrated light from quasars, as is commonly assumed, the lower limits to their  $[\text{C}/\text{H}]$  values are inferred to be between  $-2.2$  and  $-0.9$ . The relatively high metallicities of these clouds are in stark contrast with those of other similar  $N(\text{H I})$  clouds that do not show C IV absorption individually for which we inferred a mean  $[\text{C}/\text{H}] < -3.5$  from their composite spectrum. If Ly $\alpha$  clouds with  $10^{13.5} < N(\text{H I}) < 10^{14} \text{ cm}^{-2}$  have a metallicity distribution that can be approximated by a Gaussian, and if these clouds that individually show detectable C IV absorption represent the high metallicity tail of this distribution, we infer that the metallicity distribution should have a mean  $[\text{C}/\text{H}] < -4$  with a dispersion of at least 1 dex. Alternatively, the Ly $\alpha$  clouds which individually show detectable C IV absorption may have a separate origin.

We thank Francesco Haardt and Piero Madau for providing their quasar ionizing spectra in electronic form, and Gary Ferland for a copy of his CLOUDY code. We also thank all of the many people who made the Keck telescopes and their instrumentation possible. WLWS acknowledges

support from NSF grant AST95-29073. MR acknowledges support from NASA through grant number HF1075.01-94A from the Space Telescope Science Institute, which is operated by the Association of Universities for Research in Astronomy, Inc., for NASA under contract NAS5-26555.

Table 1. List of Quasars

| QSO       | $z_{em}^a$ | $V^b$ | S/N <sup>c</sup> | $\lambda$ Range <sup>d</sup> |
|-----------|------------|-------|------------------|------------------------------|
| 0100+1300 | 2.718      | 16.6  | 80-110           | 4090-4520                    |
| 0636+6801 | 3.179      | 16.5  | 80-120           | 4286-5080                    |
| 1107+4847 | 2.965      | 16.7  | 60-90            | 4235-4820                    |
| 1422+2309 | 3.629      | 16.5  | 90-160           | 4748-5627                    |
| 1425+6039 | 3.175      | 16.5  | 90-160           | 4282-5075 <sup>e</sup>       |
| 1442+2931 | 2.661      | 16.2  | 70-100           | 3900-4450 <sup>e</sup>       |
| 1700+6416 | 2.744      | 16.1  | 80-120           | 4000-4551                    |
| 1946+7658 | 3.053      | 15.9  | 80-130           | 4157-4927 <sup>e</sup>       |
| 2343+1232 | 2.579      | 17.0  | 80-110           | 3940-4351 <sup>e</sup>       |

<sup>a</sup>Adopted emission redshift for the quasar. The emission redshift is determined either from the peak of the Ly $\alpha$  emission line in the HIRES spectrum or from the highest-redshift Ly $\alpha$  absorption line observed in the spectrum, whichever is larger.

<sup>b</sup>Visual magnitude of the quasar.

<sup>c</sup>Typical S/N per 6.6 km s<sup>-1</sup> resolution element in the C IV region.

<sup>d</sup>Wavelength region used to select Ly $\alpha$  lines (see text). The lower limit is either determined by S/N requirement or by the onset of the Ly $\beta$  emission line of the quasar. The upper limit is determined by the Ly $\alpha$  emission line.

<sup>e</sup>The following spectral regions are excluded owing to damped Ly $\alpha$  absorption: 4643-4663 (Q 1425+6039), 4168-4188 (Q 1442+2931), 4660-4683 (Q1946+7658), 4155-4185 (Q 2343+1232).

Table 2. List of Ly $\alpha$  Systems

| Wavelength  | Redshift | Residual Flux | Flag |
|-------------|----------|---------------|------|
| Q 0100+1300 |          |               |      |
| 4094.153    | 2.36782  | 0.122         | 1    |
| 4100.934    | 2.37339  | 0.180         | 0    |
| 4116.390    | 2.38611  | 0.131         | 0    |
| 4119.285    | 2.38849  | 0.335         | 0    |
| 4122.550    | 2.39118  | 0.054         | 0    |
| 4127.273    | 2.39506  | 0.039         | 0    |
| 4130.397    | 2.39763  | 0.238         | 0    |
| 4132.794    | 2.39960  | 0.274         | 0    |
| 4133.622    | 2.40028  | 0.353         | 2    |
| 4143.128    | 2.40810  | 0.115         | 0    |
| 4174.774    | 2.43413  | 0.373         | 0    |
| 4177.658    | 2.43651  | 0.089         | 0    |
| 4235.625    | 2.48419  | 0.108         | 0    |
| 4258.374    | 2.50290  | 0.275         | 0    |
| 4282.304    | 2.52259  | 0.173         | 0    |
| 4285.318    | 2.52507  | 0.258         | 0    |
| 4291.262    | 2.52996  | 0.234         | 0    |
| 4301.424    | 2.53832  | 0.132         | 0    |
| 4321.220    | 2.55460  | 0.367         | 2    |
| 4354.237    | 2.58176  | 0.348         | 0    |
| 4356.169    | 2.58335  | 0.107         | 0    |
| 4357.232    | 2.58422  | 0.058         | 0    |
| 4359.902    | 2.58642  | 0.319         | 0    |
| 4361.825    | 2.58800  | 0.372         | 0    |
| 4362.708    | 2.58873  | 0.107         | 0    |
| 4380.022    | 2.60297  | 0.122         | 0    |
| 4382.571    | 2.60507  | 0.283         | 0    |
| 4396.414    | 2.61645  | 0.361         | 0    |
| 4422.073    | 2.63756  | 0.401         | 0    |
| 4428.246    | 2.64264  | 0.269         | 0    |
| Q 0636+6801 |          |               |      |

Table 2—Continued

| Wavelength | Redshift | Residual Flux | Flag |
|------------|----------|---------------|------|
| 4286.281   | 2.52586  | 0.340         | 0    |
| 4287.469   | 2.52684  | 0.210         | 0    |
| 4289.109   | 2.52818  | 0.298         | 0    |
| 4308.544   | 2.54417  | 0.307         | 0    |
| 4311.484   | 2.54659  | 0.056         | 0    |
| 4331.696   | 2.56322  | 0.098         | 2    |
| 4338.049   | 2.56844  | 0.163         | 2    |
| 4391.302   | 2.61225  | 0.106         | 0    |
| 4421.211   | 2.63685  | 0.308         | 0    |
| 4423.604   | 2.63882  | 0.036         | 0    |
| 4436.713   | 2.64960  | 0.256         | 0    |
| 4440.883   | 2.65303  | 0.204         | 0    |
| 4454.959   | 2.66461  | 0.218         | 0    |
| 4471.645   | 2.67834  | 0.203         | 0    |
| 4482.473   | 2.68724  | 0.065         | 0    |
| 4490.741   | 2.69405  | 0.151         | 0    |
| 4507.129   | 2.70753  | 0.098         | 1    |
| 4536.054   | 2.73132  | 0.853         | 1    |
| 4550.071   | 2.74285  | 0.286         | 0    |
| 4555.496   | 2.74731  | 0.042         | 0    |
| 4577.281   | 2.76523  | 0.036         | 0    |
| 4633.240   | 2.81126  | 0.219         | 2    |
| 4654.988   | 2.82915  | 0.321         | 0    |
| 4668.517   | 2.84028  | 0.124         | 0    |
| 4673.233   | 2.84416  | 0.051         | 2    |
| 4677.685   | 2.84783  | 0.208         | 0    |
| 4682.170   | 2.85151  | 0.335         | 1    |
| 4699.186   | 2.86551  | 0.154         | 0    |
| 4734.244   | 2.89435  | 0.322         | 1    |
| 4735.202   | 2.89514  | 0.339         | 3    |
| 4750.998   | 2.90813  | 0.260         | 0    |
| 4752.244   | 2.90916  | 0.097         | 1    |
| 4765.640   | 2.92018  | 0.091         | 0    |
| 4789.042   | 2.93942  | 0.114         | 0    |
| 4790.069   | 2.94027  | 0.250         | 0    |
| 4799.148   | 2.94774  | 0.144         | 0    |

Table 2—Continued

| Wavelength  | Redshift | Residual Flux | Flag |
|-------------|----------|---------------|------|
| 4800.392    | 2.94876  | 0.373         | 0    |
| 4805.420    | 2.95290  | 0.115         | 0    |
| 4827.638    | 2.97117  | 0.094         | 0    |
| 4830.792    | 2.97377  | 0.098         | 0    |
| 4840.324    | 2.98161  | 0.171         | 0    |
| 4849.687    | 2.98931  | 0.342         | 0    |
| 4857.483    | 2.99572  | 0.219         | 0    |
| 4860.029    | 2.99782  | 0.286         | 0    |
| 4890.703    | 3.02305  | 0.046         | 0    |
| 4942.479    | 3.06564  | 0.191         | 0    |
| 4962.583    | 3.08218  | 0.091         | 2    |
| 4968.049    | 3.08668  | 0.085         | 0    |
| 4970.790    | 3.08893  | 0.273         | 1    |
| 4977.749    | 3.09466  | 0.085         | 0    |
| 5005.265    | 3.11729  | 0.115         | 0    |
| 5018.773    | 3.12840  | 0.316         | 0    |
| 5033.037    | 3.14013  | 0.224         | 0    |
| 5034.347    | 3.14121  | 0.243         | 0    |
| Q 1107+4847 |          |               |      |
| 4239.687    | 2.48753  | 0.090         | 0    |
| 4256.232    | 2.50114  | 0.193         | 2    |
| 4257.300    | 2.50202  | 0.171         | 0    |
| 4299.297    | 2.53657  | 0.357         | 0    |
| 4304.639    | 2.54096  | 0.283         | 0    |
| 4347.466    | 2.57619  | 0.216         | 0    |
| 4364.434    | 2.59015  | 0.060         | 0    |
| 4380.748    | 2.60357  | 0.136         | 0    |
| 4391.133    | 2.61211  | 0.049         | 0    |
| 4398.393    | 2.61808  | 0.067         | 0    |
| 4405.924    | 2.62428  | 0.072         | 2    |
| 4426.362    | 2.64109  | 0.291         | 1    |
| 4433.019    | 2.64656  | 0.103         | 0    |
| 4438.663    | 2.65121  | 0.055         | 0    |
| 4441.819    | 2.65380  | 0.249         | 0    |

Table 2—Continued

| Wavelength            | Redshift | Residual Flux | Flag |
|-----------------------|----------|---------------|------|
| 4466.188              | 2.67385  | 0.142         | 1    |
| 4473.093              | 2.67953  | 0.287         | 0    |
| 4484.903              | 2.68924  | 0.219         | 0    |
| 4496.837              | 2.69906  | 0.310         | 0    |
| 4507.029              | 2.70744  | 0.354         | 1    |
| 4507.991              | 2.70824  | 0.383         | 2    |
| 4508.903              | 2.70899  | 0.133         | 3    |
| 4522.404              | 2.72009  | 0.064         | 0    |
| 4525.017 <sup>a</sup> | 2.72224  | 0.083         | 3    |
| 4542.543              | 2.73666  | 0.037         | 0    |
| 4544.707              | 2.73844  | 0.353         | 0    |
| 4556.674              | 2.74828  | 0.372         | 0    |
| 4558.005              | 2.74938  | 0.327         | 0    |
| 4559.907              | 2.75094  | 0.049         | 0    |
| 4568.649              | 2.75813  | 0.100         | 0    |
| 4588.396              | 2.77438  | 0.106         | 0    |
| 4593.184              | 2.77832  | 0.238         | 0    |
| 4628.681              | 2.80751  | 0.053         | 0    |
| 4639.846              | 2.81670  | 0.209         | 2    |
| 4654.944              | 2.82912  | 0.057         | 0    |
| 4668.535              | 2.84030  | 0.302         | 0    |
| 4669.555              | 2.84114  | 0.113         | 0    |
| 4682.405              | 2.85171  | 0.350         | 0    |
| 4696.837              | 2.86358  | 0.249         | 2    |
| 4709.816              | 2.87426  | 0.076         | 0    |
| 4711.625              | 2.87574  | 0.056         | 0    |
| 4739.227              | 2.89845  | 0.368         | 0    |
| 4740.343              | 2.89937  | 0.086         | 0    |
| 4759.047              | 2.91475  | 0.238         | 1    |
| 4783.936              | 2.93523  | 0.194         | 0    |
| 4809.364 <sup>a</sup> | 2.95614  | 0.044         | 3    |
| 4813.176              | 2.95928  | 0.301         | 0    |
| Q 1422+2309           |          |               |      |
| 4758.797              | 2.91455  | 0.237         | 0    |



Table 2—Continued

| Wavelength | Redshift | Residual Flux | Flag |
|------------|----------|---------------|------|
| 4766.250   | 2.92068  | 0.415         | 0    |
| 4777.278   | 2.92975  | 0.070         | 1    |
| 4790.863   | 2.94092  | 0.085         | 2    |
| 4792.363   | 2.94216  | 0.359         | 0    |
| 4811.781   | 2.95813  | 0.337         | 0    |
| 4819.289   | 2.96431  | 0.099         | 2    |
| 4821.130   | 2.96582  | 0.141         | 3    |
| 4826.135   | 2.96994  | 0.175         | 2    |
| 4840.907   | 2.98209  | 0.270         | 1    |
| 4876.051   | 3.01100  | 0.277         | 0    |
| 4880.510   | 3.01467  | 0.100         | 2    |
| 4896.016   | 3.02742  | 0.290         | 0    |
| 4899.455   | 3.03025  | 0.161         | 3    |
| 4910.845   | 3.03962  | 0.210         | 2    |
| 4917.801   | 3.04534  | 0.330         | 1    |
| 4918.696   | 3.04608  | 0.224         | 1    |
| 4919.782   | 3.04697  | 0.156         | 0    |
| 4921.119   | 3.04807  | 0.235         | 0    |
| 4930.662   | 3.05592  | 0.100         | 2    |
| 4937.801   | 3.06179  | 0.364         | 0    |
| 4948.732   | 3.07079  | 0.278         | 3    |
| 4982.914   | 3.09890  | 0.152         | 0    |
| 4987.255   | 3.10247  | 0.035         | 2    |
| 4991.231   | 3.10575  | 0.252         | 2    |
| 4993.338   | 3.10748  | 0.315         | 0    |
| 5004.771   | 3.11688  | 0.350         | 0    |
| 5017.920   | 3.12770  | 0.045         | 2    |
| 5020.106   | 3.12950  | 0.199         | 3    |
| 5157.707   | 3.24269  | 0.045         | 0    |
| 5166.664   | 3.25005  | 0.139         | 2    |
| 5170.188   | 3.25295  | 0.226         | 0    |
| 5187.813   | 3.26745  | 0.113         | 0    |
| 5201.190   | 3.27846  | 0.038         | 0    |
| 5208.194   | 3.28422  | 0.272         | 2    |
| 5211.599   | 3.28702  | 0.298         | 0    |
| 5212.832   | 3.28803  | 0.097         | 0    |

Table 2—Continued

| Wavelength            | Redshift | Residual Flux | Flag |
|-----------------------|----------|---------------|------|
| 5237.367              | 3.30821  | 0.382         | 0    |
| 5241.231              | 3.31139  | 0.220         | 2    |
| 5249.536 <sup>a</sup> | 3.31822  | 0.080         | 1    |
| 5250.509              | 3.31903  | 0.192         | 0    |
| 5279.110              | 3.34255  | 0.074         | 0    |
| 5286.269              | 3.34844  | 0.314         | 0    |
| 5291.105              | 3.35242  | 0.379         | 0    |
| 5315.959              | 3.37286  | 0.341         | 2    |
| 5319.197              | 3.37553  | 0.048         | 2    |
| 5322.354              | 3.37812  | 0.199         | 0    |
| 5341.464              | 3.39384  | 0.113         | 1    |
| 5370.738              | 3.41792  | 0.146         | 1    |
| 5387.182              | 3.43145  | 0.285         | 2    |
| 5395.701              | 3.43846  | 0.341         | 3    |
| 5411.299 <sup>a</sup> | 3.45129  | 0.053         | 3    |
| 5423.721              | 3.46151  | 0.286         | 0    |
| 5432.508              | 3.46873  | 0.163         | 2    |
| 5439.274              | 3.47430  | 0.066         | 0    |
| 5484.907              | 3.51184  | 0.124         | 0    |
| 5494.495              | 3.51973  | 0.085         | 0    |
| 5509.467              | 3.53204  | 0.133         | 2    |
| 5554.169              | 3.56881  | 0.238         | 0    |
| 5561.464              | 3.57481  | 0.155         | 0    |
| 5562.494              | 3.57566  | 0.243         | 0    |
| 5585.622              | 3.59469  | 0.248         | 1    |
| 5601.092              | 3.60741  | 0.300         | 0    |
| 5617.280              | 3.62073  | 0.085         | 2    |
| 5620.783 <sup>a</sup> | 3.62361  | 0.082         | 3    |
| 5621.720 <sup>a</sup> | 3.62438  | 0.088         | 3    |
| 5627.097              | 3.62880  | 0.151         | 3    |
| Q 1425+6039           |          |               |      |
| 4286.917              | 2.52638  | 0.041         | 2    |
| 4295.367              | 2.53333  | 0.372         | 0    |
| 4318.305              | 2.55220  | 0.212         | 0    |

Table 2—Continued

| Wavelength            | Redshift | Residual Flux | Flag |
|-----------------------|----------|---------------|------|
| 4329.535              | 2.56144  | 0.241         | 0    |
| 4339.103              | 2.56931  | 0.213         | 0    |
| 4412.140              | 2.62939  | 0.362         | 0    |
| 4419.553              | 2.63549  | 0.117         | 0    |
| 4421.911              | 2.63743  | 0.195         | 0    |
| 4437.250              | 2.65004  | 0.242         | 0    |
| 4452.923              | 2.66294  | 0.211         | 1    |
| 4486.830              | 2.69083  | 0.145         | 1    |
| 4519.021              | 2.71731  | 0.311         | 3    |
| 4534.893              | 2.73037  | 0.368         | 0    |
| 4562.383              | 2.75298  | 0.057         | 3    |
| 4629.492              | 2.80818  | 0.060         | 1    |
| 4663.989              | 2.83656  | 0.084         | 1    |
| 4664.949              | 2.83735  | 0.230         | 1    |
| 4671.281              | 2.84256  | 0.111         | 1    |
| 4684.343              | 2.85330  | 0.088         | 0    |
| 4735.381              | 2.89528  | 0.254         | 0    |
| 4736.249              | 2.89600  | 0.056         | 0    |
| 4739.185              | 2.89841  | 0.211         | 2    |
| 4740.526              | 2.89952  | 0.338         | 1    |
| 4744.760              | 2.90300  | 0.305         | 2    |
| 4767.407              | 2.92163  | 0.113         | 0    |
| 4774.520              | 2.92748  | 0.127         | 0    |
| 4796.577              | 2.94562  | 0.128         | 0    |
| 4798.067              | 2.94685  | 0.232         | 0    |
| 4806.079              | 2.95344  | 0.277         | 0    |
| 4808.011              | 2.95503  | 0.236         | 1    |
| 4907.598              | 3.03695  | 0.271         | 2    |
| 4911.555              | 3.04020  | 0.260         | 1    |
| 4923.173              | 3.04976  | 0.344         | 3    |
| 4929.528              | 3.05499  | 0.107         | 1    |
| 4947.206              | 3.06953  | 0.359         | 1    |
| 4951.747              | 3.07327  | 0.216         | 3    |
| 4952.611 <sup>a</sup> | 3.07398  | 0.160         | 3    |
| 4971.342              | 3.08938  | 0.222         | 3    |
| 4999.012              | 3.11214  | 0.223         | 0    |

Table 2—Continued

| Wavelength            | Redshift | Residual Flux | Flag |
|-----------------------|----------|---------------|------|
| 5023.327              | 3.13215  | 0.079         | 1    |
| Q 1442+2931           |          |               |      |
| 3903.794              | 2.21123  | 0.285         | 0    |
| 3905.104              | 2.21231  | 0.356         | 0    |
| 3971.901              | 2.26725  | 0.273         | 0    |
| 3973.539              | 2.26860  | 0.350         | 0    |
| 3978.611              | 2.27277  | 0.320         | 2    |
| 3999.285              | 2.28978  | 0.367         | 0    |
| 4032.404              | 2.31702  | 0.261         | 0    |
| 4066.457              | 2.34503  | 0.103         | 0    |
| 4075.212              | 2.35224  | 0.387         | 0    |
| 4113.835              | 2.38401  | 0.169         | 2    |
| 4154.397              | 2.41737  | 0.362         | 0    |
| 4159.561              | 2.42162  | 0.092         | 2    |
| 4197.781              | 2.45306  | 0.123         | 0    |
| 4199.317              | 2.45432  | 0.193         | 0    |
| 4202.369              | 2.45683  | 0.274         | 0    |
| 4210.112              | 2.46320  | 0.088         | 0    |
| 4222.104              | 2.47307  | 0.120         | 3    |
| 4225.344              | 2.47573  | 0.349         | 0    |
| 4230.729              | 2.48016  | 0.386         | 1    |
| 4234.958 <sup>a</sup> | 2.48364  | 0.383         | 3    |
| 4237.895              | 2.48606  | 0.105         | 0    |
| 4242.205              | 2.48960  | 0.071         | 1    |
| 4248.379              | 2.49468  | 0.261         | 0    |
| 4273.131              | 2.51504  | 0.266         | 0    |
| 4308.993              | 2.54454  | 0.245         | 0    |
| 4318.667              | 2.55250  | 0.246         | 0    |
| 4323.667              | 2.55661  | 0.133         | 0    |
| 4341.328              | 2.57114  | 0.233         | 1    |
| 4348.721              | 2.57722  | 0.125         | 0    |
| 4367.699              | 2.59283  | 0.198         | 0    |
| 4378.564              | 2.60177  | 0.389         | 0    |
| 4390.083              | 2.61125  | 0.316         | 2    |

Table 2—Continued

| Wavelength  | Redshift | Residual Flux | Flag |
|-------------|----------|---------------|------|
| Q 1700+6416 |          |               |      |
| 4055.872    | 2.33633  | 0.191         | 0    |
| 4071.267    | 2.34899  | 0.092         | 1    |
| 4079.972    | 2.35615  | 0.191         | 0    |
| 4093.271    | 2.36709  | 0.029         | 1    |
| 4103.101    | 2.37518  | 0.237         | 1    |
| 4127.951    | 2.39562  | 0.054         | 1    |
| 4140.000    | 2.40553  | 0.286         | 0    |
| 4170.336    | 2.43048  | 0.325         | 0    |
| 4185.509    | 2.44297  | 0.296         | 1    |
| 4216.740    | 2.46866  | 0.299         | 0    |
| 4218.814    | 2.47036  | 0.212         | 0    |
| 4220.503    | 2.47175  | 0.161         | 1    |
| 4233.472    | 2.48242  | 0.328         | 0    |
| 4262.720    | 2.50648  | 0.160         | 0    |
| 4267.122    | 2.51010  | 0.115         | 0    |
| 4282.338    | 2.52262  | 0.243         | 0    |
| 4336.106    | 2.56684  | 0.287         | 0    |
| 4367.674    | 2.59281  | 0.106         | 2    |
| 4370.138    | 2.59484  | 0.147         | 1    |
| 4374.728    | 2.59861  | 0.330         | 0    |
| 4381.077    | 2.60384  | 0.045         | 1    |
| 4401.184    | 2.62038  | 0.293         | 0    |
| 4422.048    | 2.63754  | 0.204         | 0    |
| 4430.501    | 2.64449  | 0.208         | 0    |
| 4432.457    | 2.64610  | 0.235         | 0    |
| 4433.164    | 2.64668  | 0.118         | 0    |
| 4436.012    | 2.64903  | 0.264         | 0    |
| 4438.243    | 2.65086  | 0.269         | 0    |
| 4475.114    | 2.68119  | 0.168         | 0    |
| 4484.028    | 2.68852  | 0.291         | 0    |
| 4500.091    | 2.70174  | 0.077         | 0    |
| 4510.327    | 2.71016  | 0.047         | 2    |
| 4527.784    | 2.72452  | 0.275         | 0    |

Table 2—Continued

| Wavelength  | Redshift | Residual Flux | Flag |
|-------------|----------|---------------|------|
| 4537.776    | 2.73274  | 0.322         | 0    |
| 4551.758    | 2.74424  | 0.180         | 0    |
| Q 1946+7658 |          |               |      |
| 4215.363    | 2.46752  | 0.326         | 1    |
| 4216.741    | 2.46866  | 0.316         | 0    |
| 4233.834    | 2.48272  | 0.159         | 1    |
| 4254.062    | 2.49936  | 0.325         | 3    |
| 4272.777    | 2.51475  | 0.087         | 0    |
| 4310.893    | 2.54610  | 0.335         | 0    |
| 4322.006    | 2.55525  | 0.395         | 0    |
| 4345.969    | 2.57496  | 0.070         | 0    |
| 4348.446    | 2.57700  | 0.190         | 0    |
| 4354.806    | 2.58223  | 0.039         | 0    |
| 4358.269    | 2.58508  | 0.200         | 0    |
| 4381.860    | 2.60448  | 0.269         | 2    |
| 4388.862    | 2.61024  | 0.313         | 1    |
| 4391.371    | 2.61230  | 0.337         | 0    |
| 4397.191    | 2.61709  | 0.121         | 0    |
| 4403.181    | 2.62202  | 0.186         | 0    |
| 4406.600    | 2.62483  | 0.330         | 1    |
| 4421.906    | 2.63742  | 0.127         | 2    |
| 4425.030    | 2.63999  | 0.051         | 2    |
| 4439.273    | 2.65171  | 0.145         | 0    |
| 4445.566    | 2.65688  | 0.085         | 0    |
| 4460.339    | 2.66904  | 0.050         | 1    |
| 4464.265    | 2.67227  | 0.178         | 0    |
| 4489.117    | 2.69271  | 0.228         | 0    |
| 4500.549    | 2.70211  | 0.200         | 0    |
| 4506.008    | 2.70660  | 0.139         | 0    |
| 4531.280    | 2.72739  | 0.367         | 0    |
| 4537.618    | 2.73261  | 0.304         | 1    |
| 4570.602    | 2.75974  | 0.060         | 0    |
| 4578.117    | 2.76592  | 0.306         | 0    |
| 4593.453    | 2.77854  | 0.099         | 0    |

Table 2—Continued

| Wavelength            | Redshift | Residual Flux | Flag |
|-----------------------|----------|---------------|------|
| 4619.984              | 2.80036  | 0.244         | 1    |
| 4633.098              | 2.81115  | 0.367         | 0    |
| 4647.124              | 2.82269  | 0.173         | 0    |
| 4656.047              | 2.83002  | 0.199         | 1    |
| 4692.409              | 2.85994  | 0.080         | 0    |
| 4749.612              | 2.90699  | 0.306         | 2    |
| 4753.097              | 2.90986  | 0.107         | 2    |
| 4759.734              | 2.91532  | 0.291         | 1    |
| 4780.079              | 2.93205  | 0.091         | 0    |
| 4818.925              | 2.96401  | 0.387         | 0    |
| 4836.081              | 2.97812  | 0.177         | 2    |
| 4842.774              | 2.98363  | 0.127         | 0    |
| 4846.812              | 2.98695  | 0.273         | 2    |
| 4871.646              | 3.00738  | 0.184         | 0    |
| 4881.021              | 3.01509  | 0.235         | 0    |
| 4901.713              | 3.03211  | 0.245         | 2    |
| 4904.279 <sup>a</sup> | 3.03422  | 0.090         | 3    |
| Q 2343+1232           |          |               |      |
| 3965.490              | 2.26198  | 0.084         | 1    |
| 3982.626              | 2.27607  | 0.065         | 0    |
| 3983.400              | 2.27671  | 0.113         | 0    |
| 3993.207              | 2.28478  | 0.051         | 2    |
| 4015.365              | 2.30300  | 0.129         | 0    |
| 4019.717              | 2.30659  | 0.278         | 0    |
| 4071.661              | 2.34931  | 0.150         | 0    |
| 4112.756              | 2.38312  | 0.310         | 1    |
| 4150.644              | 2.41428  | 0.147         | 0    |
| 4195.085              | 2.45084  | 0.331         | 2    |
| 4207.765              | 2.46127  | 0.056         | 0    |
| 4209.998              | 2.46311  | 0.189         | 2    |
| 4210.993              | 2.46393  | 0.104         | 0    |
| 4236.032              | 2.48452  | 0.373         | 0    |
| 4237.870              | 2.48604  | 0.375         | 0    |
| 4239.561              | 2.48743  | 0.198         | 2    |

Table 2—Continued

| Wavelength            | Redshift | Residual Flux | Flag |
|-----------------------|----------|---------------|------|
| 4248.781              | 2.49501  | 0.305         | 0    |
| 4257.533 <sup>a</sup> | 2.50221  | 0.106         | 1    |

<sup>a</sup>This system shows detectable C IV absorption.



### Notes to Table 3

<sup>a</sup> Column density (logarithmic) of H I and C IV based on Voigt profile fits to the Ly $\alpha$  line and the C IV doublet.

<sup>b</sup> Temperature of the gas implied by the width of the Ly $\alpha$  and the C IV absorption lines.

<sup>c</sup> Metallicity of the gas assuming the gas is photoionized. For intervening systems the photoionization results using the  $\alpha = -1.8$  Haardt & Madau (1996) quasar spectrum including intervening opacity are adopted. For associated systems the photoionization results using the unabsorbed  $\alpha = -1.8$  quasar spectrum of Haardt & Madau (1996) are used.

<sup>d</sup> Metallicity of the gas assuming the gas is collisionally ionized and is in thermal and ionization equilibria.

<sup>e</sup> Type of the absorption system. All intervening systems are more than 10,000 km s<sup>-1</sup> away from the emission redshift of the quasars, and all associated systems are within 3000 km s<sup>-1</sup> of the quasar emission redshifts.

<sup>f</sup> This system is within 50 km s<sup>-1</sup> of another strong Ly $\alpha$  absorption and would otherwise not be included in the Ly $\alpha$  sample in Table 2.

<sup>g</sup> The C IV absorption at this redshift has two components. The values given are for the stronger component. The weaker component adds only 18% to the C IV column density.

<sup>h</sup> Both the Ly $\alpha$  and C IV absorption require two components of comparable column densities to fit. The values given are for the sum of the two.

<sup>i</sup> The C IV  $\lambda 1548$  absorption is blended with the C IV  $\lambda 1550$  absorption at  $z = 3.06702$ . The values are obtained after deblending.

<sup>j</sup> The Ly $\alpha$  lines of these two systems are very close to each other and require 3 components to fit. It is impossible to determine the N(H I) of each system. The values listed are for the sum of the two systems (3 components).

<sup>k</sup> The Ly $\alpha$  line requires two closely spaced components of comparable column densities to fit. The values given are for the sum of the two. The formal  $b$  values of the components are 13.5 and 13.9 km s<sup>-1</sup>, implying  $\log T < 4.5$  and 4.8 respectively.

<sup>l</sup> The C IV absorption at this redshift has two components. The values given are for the stronger component. The weaker component adds only 30% to the C IV column density.

Table 3. Ly $\alpha$  Systems with Metals

| QSO                              | $z_{abs}$            | N(H I) <sup>a</sup> | N(C IV) <sup>a</sup> | log T(H I) <sup>b</sup> | log T(C IV) <sup>b</sup> | [C/H] <sub>P</sub> <sup>c</sup> | [C/H] <sub>C</sub> <sup>d</sup> |
|----------------------------------|----------------------|---------------------|----------------------|-------------------------|--------------------------|---------------------------------|---------------------------------|
| Associated Systems <sup>e</sup>  |                      |                     |                      |                         |                          |                                 |                                 |
| 1107+4847                        | 2.95614              | 13.99               | 12.09                | < 4.6                   | < 5.0                    | > -1.85                         | > -2.76                         |
| 1422+2309                        | 3.58914 <sup>f</sup> | 13.25               | 12.55                | < 4.2                   | < 5.3                    | > -0.67                         | > -1.56                         |
|                                  | 3.62361              | 13.78               | 13.45 <sup>g</sup>   | < 4.4                   | < 4.9 <sup>g</sup>       | > -0.28                         | > -1.19                         |
|                                  | 3.62438              | 13.99 <sup>h</sup>  | 13.59 <sup>h</sup>   | ... <sup>h</sup>        | ... <sup>h</sup>         | > -0.35                         | > -1.26                         |
| 1425+6039                        | 3.15341 <sup>f</sup> | 14.40 <sup>j</sup>  | 13.06 <sup>j</sup>   | ... <sup>j</sup>        | < 5.8                    | > -1.29                         | > -2.20                         |
|                                  | 3.15401 <sup>f</sup> | ... <sup>j</sup>    | ... <sup>j</sup>     | ... <sup>j</sup>        | < 5.5                    | ...                             | ...                             |
| 1946+7658                        | 3.03422              | 14.06 <sup>k</sup>  | 12.43                | ... <sup>k</sup>        | < 5.2                    | > -1.58                         | > -2.49                         |
| 2343+1232                        | 2.56892 <sup>f</sup> | 13.49               | 13.47                | < 4.4                   | < 4.6                    | > +0.03                         | > -0.88                         |
|                                  | 2.56940 <sup>f</sup> | 13.58               | 13.36 <sup>l</sup>   | < 4.3                   | < 4.6 <sup>l</sup>       | > -0.17                         | > -1.08                         |
| Intervening Systems <sup>e</sup> |                      |                     |                      |                         |                          |                                 |                                 |
| 1107+4847                        | 2.72224              | 13.74               | 12.98                | < 4.3                   | < 4.4                    | > -1.10                         | > -1.62                         |
| 1422+2309                        | 3.13247 <sup>f</sup> | 13.71               | 12.47                | < 4.9                   | < 5.8                    | > -1.58                         | > -2.10                         |
|                                  | 3.31822              | 13.96               | 12.47                | < 4.7                   | < 5.9                    | > -1.83                         | > -2.35                         |
|                                  | 3.45129              | 13.99               | 12.69                | < 4.6                   | < 5.5                    | > -1.64                         | > -2.16                         |
| 1425+6039                        | 3.07398              | 13.66               | 12.44 <sup>i</sup>   | < 4.4                   | < 4.6 <sup>i</sup>       | > -1.56                         | > -2.08                         |
| 1442+2931                        | 2.48364              | 13.30               | 12.75                | < 4.2                   | < 4.3                    | > -0.89                         | > -1.41                         |
| 2343+1232                        | 2.50221              | 13.78               | 11.95                | < 4.4                   | < 5.2                    | > -2.17                         | > -2.69                         |

Table 4. Results based on Composite Spectra

| Sample <sup>a</sup> | No. Systems <sup>b</sup> | $\langle z \rangle^b$ | S/N <sup>c</sup> | $\log \langle N(\text{H I}) \rangle^d$ | $w_r(1548)^e$                 | $\log \langle N(\text{C IV}) \rangle^f$ | [C/H] <sup>g</sup> |
|---------------------|--------------------------|-----------------------|------------------|--|-------------------------------|---|--------------------|
| A                   | 282                      | 2.748                 | 1860             | 13.75                                  | $< 0.088 \text{ m}\text{\AA}$ | $< 10.34$                               | $< -3.49$          |
| B                   | 156                      | 2.727                 | 1390             | 13.63                                  | $< 0.113 \text{ m}\text{\AA}$ | $< 10.45$                               | $< -3.15$          |
| C                   | 126                      | 2.774                 | 1240             | 13.88                                  | $< 0.134 \text{ m}\text{\AA}$ | $< 10.52$                               | $< -3.55$          |
| D                   | 153                      | 2.526                 | 1300             | 13.75                                  | $< 0.120 \text{ m}\text{\AA}$ | $< 10.47$                               | $< -3.36$          |
| E                   | 129                      | 3.012                 | 1330             | 13.75                                  | $< 0.123 \text{ m}\text{\AA}$ | $< 10.48$                               | $< -3.35$          |
| F                   | 27                       | 2.846                 | 600              | 13.75                                  | $< 0.251 \text{ m}\text{\AA}$ | $< 10.79$                               | $< -3.04$          |
| G                   | 12                       | 3.030                 | 380              | 13.75                                  | $< 0.499 \text{ m}\text{\AA}$ | $< 11.09$                               | $< -2.74$          |

<sup>a</sup>Samples are defined in section 3.3.

<sup>b</sup>Number of Ly $\alpha$  systems used to form the composite spectrum and the mean redshift of the sample.

<sup>c</sup>The S/N per 6.6 km/s resolution element near the C IV  $\lambda 1548$  line in the composite spectrum, calculated from the formal error spectrum.

<sup>d</sup>Mean H I column density of the sample estimated from the column density distribution  $f(N) \propto N^{-1.5}$ .

<sup>e</sup>Upper limit on the rest-frame equivalent width of C IV  $\lambda 1548$  at the 95.5% confidence level based on the results of Monte Carlo simulations.

<sup>f</sup>Upper limit on N(C IV) at the 95.5% confidence level, derived from the equivalent width limit in column 5 assuming linear part of curve of growth.

<sup>g</sup>Upper limit on [C/H] at the 95.5% confidence level; see section 3.2 for details.

## REFERENCES

- Barlow, T.A., & Tytler, D. 1997, *AJ*, submitted
- Blades, J.C. 1988, in *QSO Absorption Lines: Probing the Universe*, eds. J.C. Blades, D. Turnshek, & C.A. Norman (Cambridge University Press), 147
- Cen, R., Miralda-Escude, J., Ostriker, J.P., & Rauch, M. 1994, *ApJ*, 437, L9
- Cowie, L.L., Songaila, A., Kim, T.-S., & Hu, E.M. 1995, *AJ*, 109, 1522
- Ferland, G.J. 1996, *Hazy*, a Brief Introduction to CLOUDY 90, University of Kentucky Physics Department Internal Report
- Foltz, C.B., Chaffee, F.H. Jr., Weymann, R.J., & Anderson, S.F. 1988, in *QSO Absorption Lines: Probing the Universe*, eds. Blades, Turnshek, and Norman (Cambridge University Press), 53
- Gnedin, Y.N., Ostriker J.P. 1997, *ApJ*, 486, 581
- Haardt, F., & Madau, P. 1996, *ApJ*, 461, 20
- Hamann, F., 1997, *ApJS*, 109, 279
- Hellsten, U., Dave, R., Hernquist L., Weinberg D.H., Katz, N. 1997, *ApJ*, 487, 482
- Hernquist, L., Katz, N., Weinberg, D.H., & Miralda-Escude, J. 1996, *ApJ*, 457, L51
- Hu, E.M., Kim, T.-S., Cowie, L.L., Songaila, A., & Rauch, M. 1995, *AJ*, 110, 1526
- Kirkman, D., & Tytler, D. 1997, *ApJ*, 484, 672
- Laor, A., Fiore, F., Elvis, M., Wilkes, B.J., McDowell, J.C. 1997, *ApJ*, 477, 93
- Lu, L. 1991, *ApJ*, 379, 99
- Lu, L., & Savage, B.D. 1993, *ApJ*, 403, 127
- Lu, L., Sargent, W.L.W., & Barlow, T.A. 1997, in *Cosmic Chemical Evolution*, IAU Symp. 187, in press
- Lu, L., Sargent, W.L.W., Barlow, T.A., Churchill, C.W., & Vogt, S.S. 1996, *ApJS*, 107, 475 (b)
- Lu, L., Sargent, W.L.W., & Womble, D.S., & Takada-Hidai, M. 1996, *ApJ*, 472, 509 (a)
- Meyer, D.M., & York, D.G. 1987, *ApJ*, 315, L5
- Miralda-Escude, J., Cen, R., Ostriker, J.P., & Rauch, M. 1996, *ApJ*, 471, 582
- Murakami, I., Yamashita, K., 1997, *Proceedings of the 13th IAP Colloquium: Structure and Evolution of the IGM from QSO Absorption Systems*.
- Norris, J., Hartwick, F.D.A., & Peterson, B.A. 1983, *ApJ*, 273, 450
- Ostriker, J.P., & Gnedin, N.Y. 1996, *ApJ*, 472, L63
- Petitjean, P., Mucket, J.P., & Kates, R.E. 1995, *A&A*, 295, L9
- Petitjean, P., Rauch, M., & Carswell, R.F. 1994, *A&A*, 291, 29

- Pettini, M., Smith, L.J., King, D.L., & Hunstead, R.W. 1997, *ApJ*, 486, 665
- Rauch, M., Haehnelt, M.G., & Steinmetz, M. 1997, *ApJ*, 481, 601
- Rauch, M., Sargent, W.L.W., Womble, D.S., & Barlow, T.A. 1996, *ApJ*, 467, L5
- Sargent, W.L.W., Young, P., Boksenberg, A., & Tytler, D. 1980, *ApJS*, 42, 41
- Savaglio, S., D’Odorico, S., & Moller, P. 1994, *A&A*, 281, 331
- Songaila, A., & Cowie, L.L. 1996, *AJ*, 112, 335
- Steidel, C.C. 1990, *ApJS*, 74, 37
- Steinmetz, M. 1997, Proceedings of the 13th IAP Colloquium: Structure and Evolution of the IGM from QSO Absorption Systems, in press
- Sutherland, R.S., & Dopita, M.A. 1993, *ApJS*, 88, 253
- Tripp, T.M., Lu, L., & Savage, B.D. 1996, *ApJS*, 102, 239
- Tytler, D., & Fan, X.-M. 1994, *ApJ*, 424, L87
- Tytler, D., Fan, X.-M., Burles, S., Cottrell, L., Davis, C., Kirkman, D., & Zuo, L. 1995, in *QSO Absorption Lines*, ed. G.Meylan (Springer-Verlag), 289
- Vogt, S. 1992, in *High Resolution Spectroscopy with the VLT*, ed. M.-H. Ulrich (Garching:ESO), 223
- Williger, G.M., Carswell, R.F., Webb, J.K., Boksenberg, A., & Smith, M.G. 1989, *MNRAS*, 237, 635
- Wolfe, A.M. 1988, in *QSO Absorption Lines: Probing the Universe*, eds. Blades, Turnshek, and Norman (Cambridge University Press), 297
- Zhang, Y., Anninos, P., & Norman, M.L. 1995, *ApJ*, 453, L57
- Zheng, W., Kriss, G.A., Telfer, R.C., Crimes, J.P., & Davidsen, A.F., 1998, *ApJ*, 492, 855

**Figure 1** - Distribution of Ly $\alpha$  clouds in the spectrum of Q 1946+7658 that are included in our sample of Ly $\alpha$  systems based on selection by optical depth (Table 2). The actual N(H I) of the clouds are from Voigt profile fitting by Kirkman & Tytler (1997). The dashed line, scaled arbitrarily to roughly match the observed distribution, indicates the expected distribution from the known column density distribution of  $f(N) \propto N^{-1.5}$ . It is seen that the N(H I) of most of the Ly $\alpha$  lines selected falls within the desired range of  $10^{13.5} < N(\text{H I}) < 10^{14} \text{ cm}^{-2}$ .

**Figure 2** - Profiles of Ly $\alpha$  and C IV  $\lambda$ 1548, 1550 in the 16 Ly $\alpha$  systems with detectable C IV absorption (Table 3). Note that 6 of the systems form close redshift pairs and are displayed in 3 panels. The type of the absorption systems (Table 3) are indicated: “I” for intervening and “A” for associated. The profiles are shown in velocity space in the rest frame of the absorbers.

**Figure 3** - Composite spectrum for Sample A. The spectrum is shown in velocity space relative to C IV  $\lambda$ 1548.20 Å. The velocity bin size is 3.3 km s $^{-1}$ . The two vertical lines mark the expected position of the C IV  $\lambda$ 1548.20, 1550.77 absorption. The smooth curve is the fitted continuum, which includes the absorption by a C IV doublet with  $b = 10 \text{ km s}^{-1}$  and with  $w_r(1548)$  equal to the  $4\sigma$  upper limit.

**Figure 4** - Metallicity as a function of H I column density for quasar absorption line systems. The box labeled “DLA” is for damped Ly $\alpha$  systems using [Fe/H] as the metallicity indicator (Lu et al 1996). The box outlined with dotted lines indicates the metallicity distribution of damped Ly $\alpha$  systems if [Zn/H] is used as a metallicity indicator instead (Pettini et al 1997). The box labeled “LLS” is for Lyman limit systems studied by Steidel (1990). The box labeled “Ly $\alpha$ ” is for Ly $\alpha$  clouds with  $N(\text{H I}) > 10^{14.5} \text{ cm}^{-2}$  studied by Cowie et al (1995), Tytler et al (1995), Songaila & Cowie (1996) and Rauch et al (1997). The sizes of the boxes roughly indicate the spread in the metallicity distribution (vertical direction) and the range of N(H I) (horizontal direction). For the Ly $\alpha$  clouds, the spread in metallicity is not well documented in any of the references quoted; a spread of 1 dex is assumed. The upper limit at the lowest column density is from this study.

**Figure 5** - Constraints on the metallicity distribution of Ly $\alpha$  clouds. The meaning of this figure is explained in section 4.2.

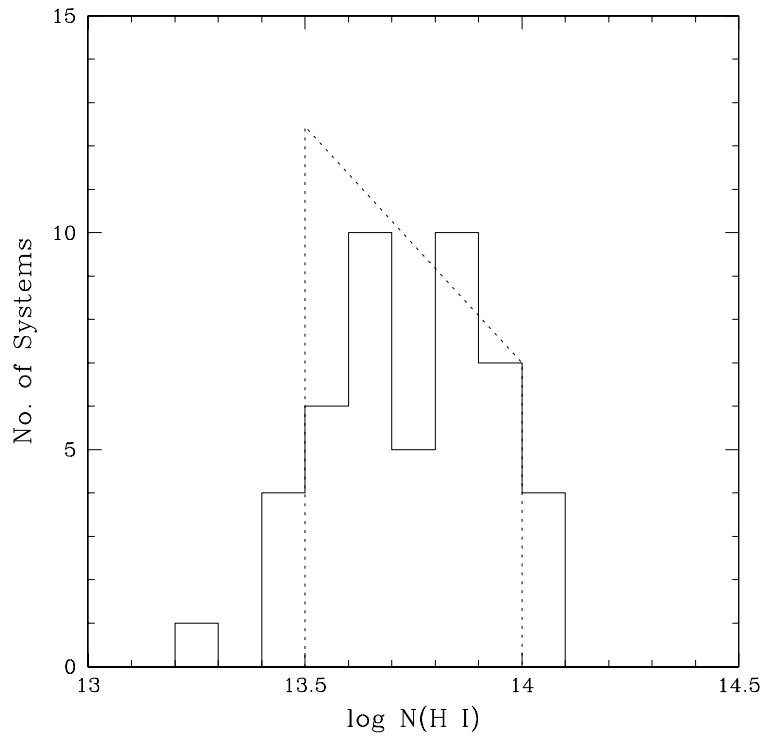


Fig. 1.—

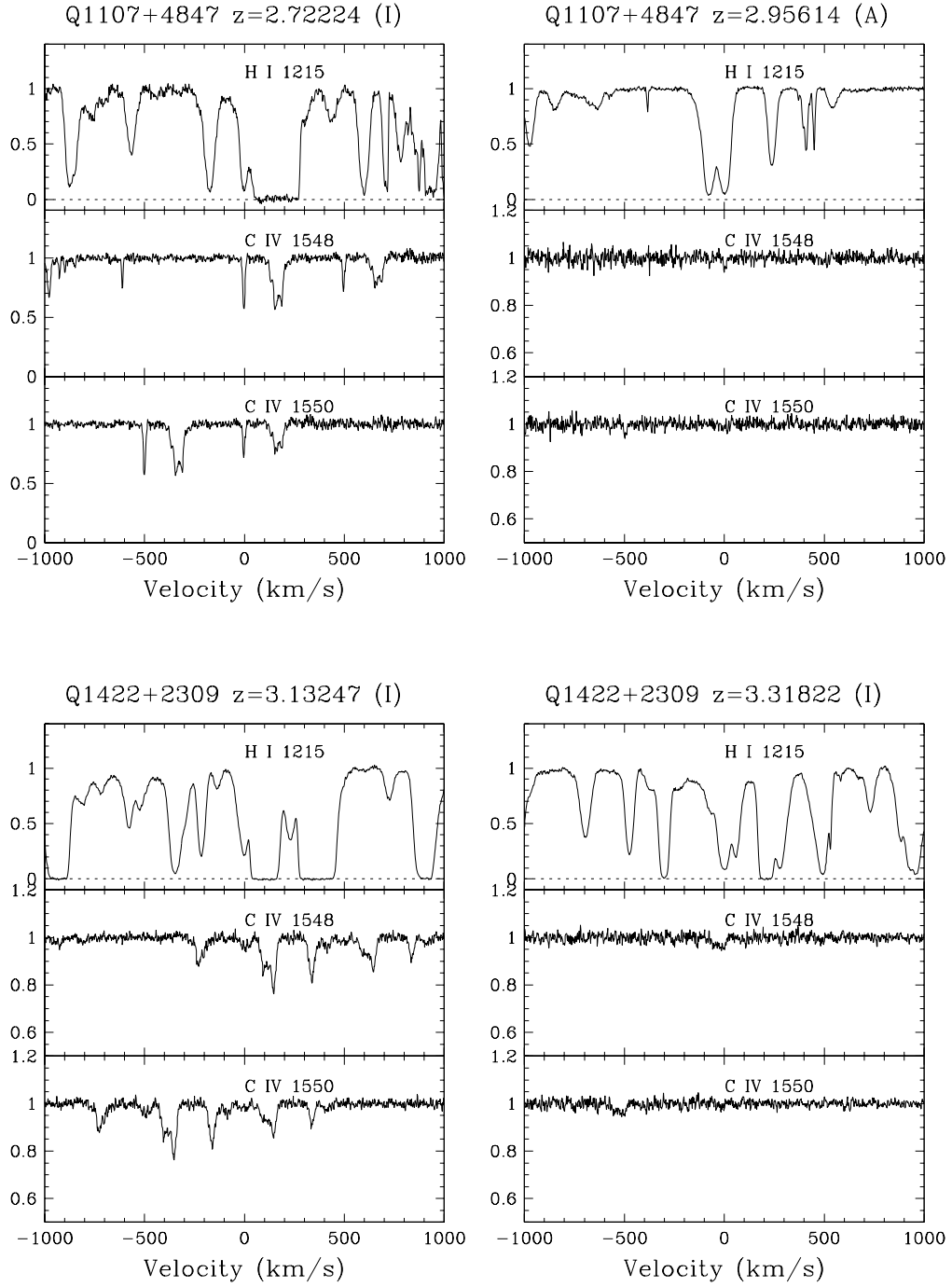
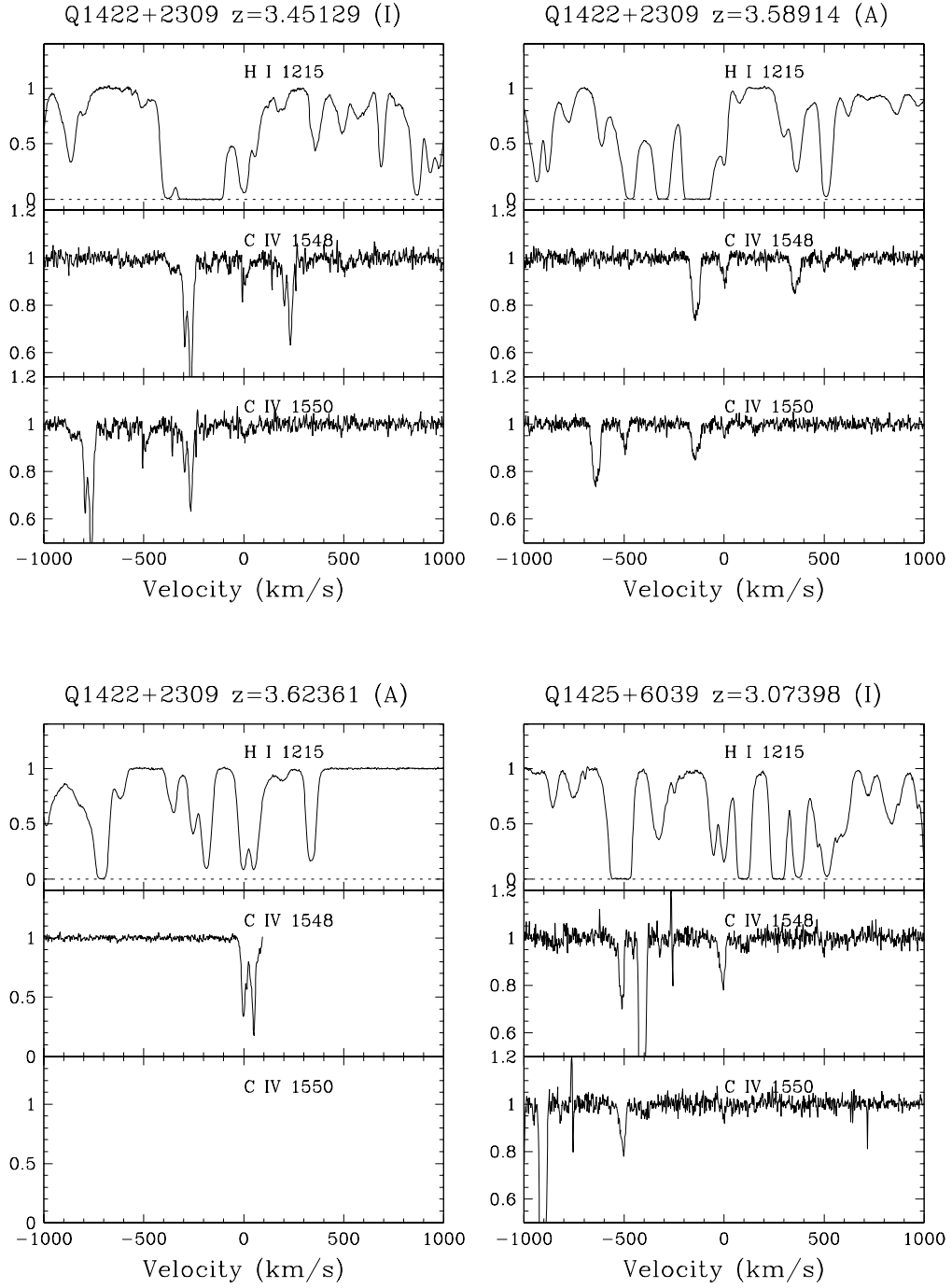
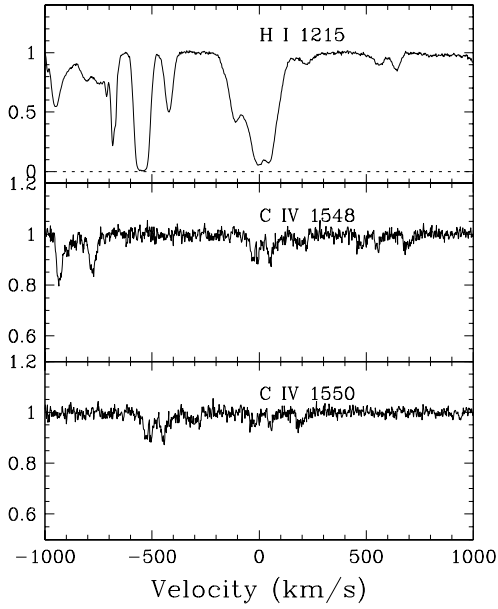


Fig. 2.—

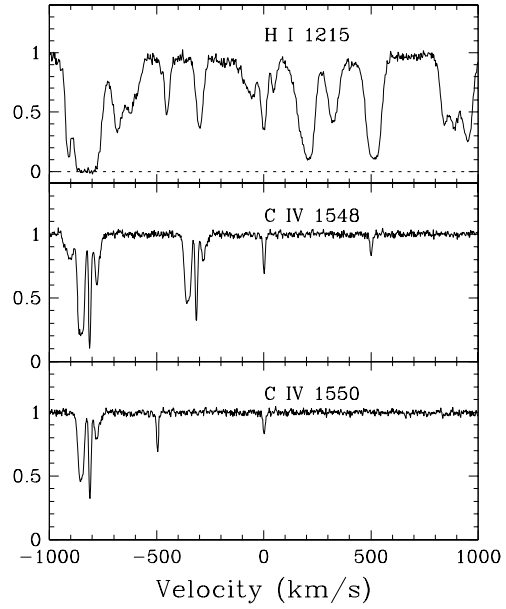




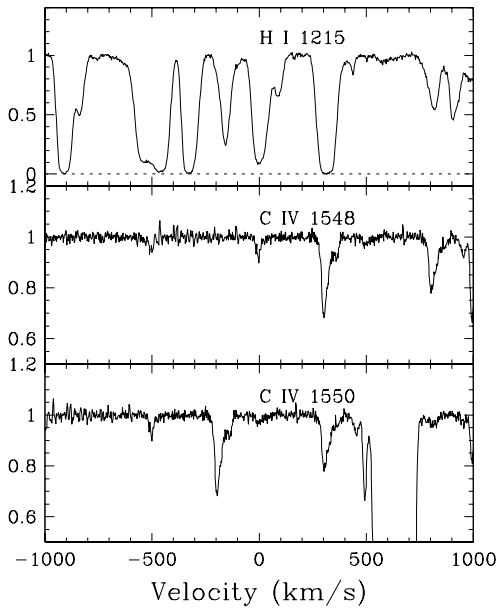
Q1425+6039  $z=3.15341$  (A)



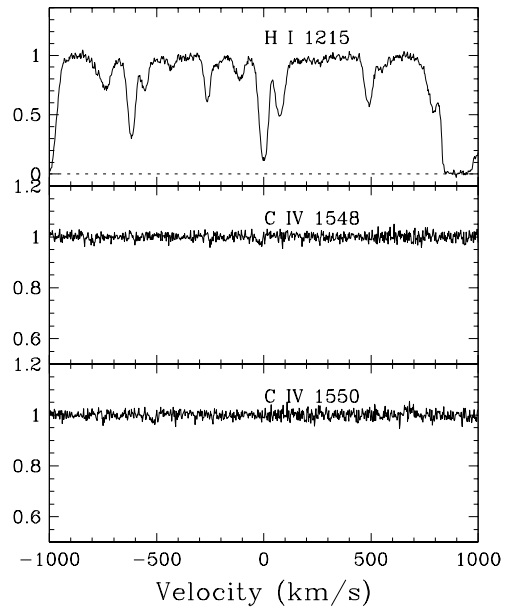
Q1442+2931  $z=2.48364$  (I)

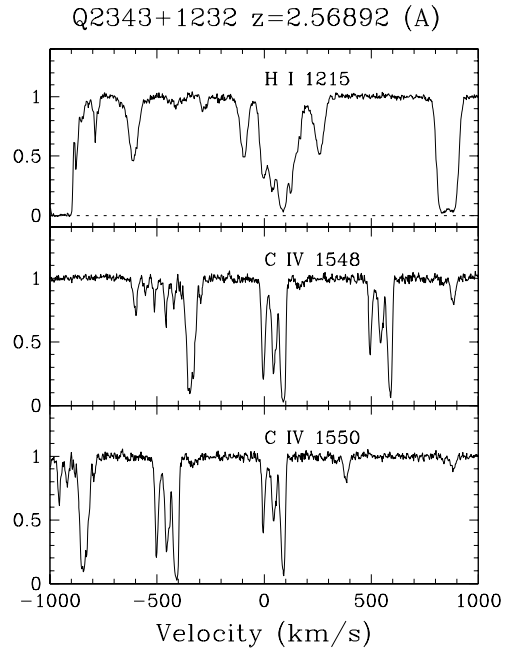


Q1946+7658  $z=3.03422$  (A)



Q2343+1232  $z=2.50221$  (I)





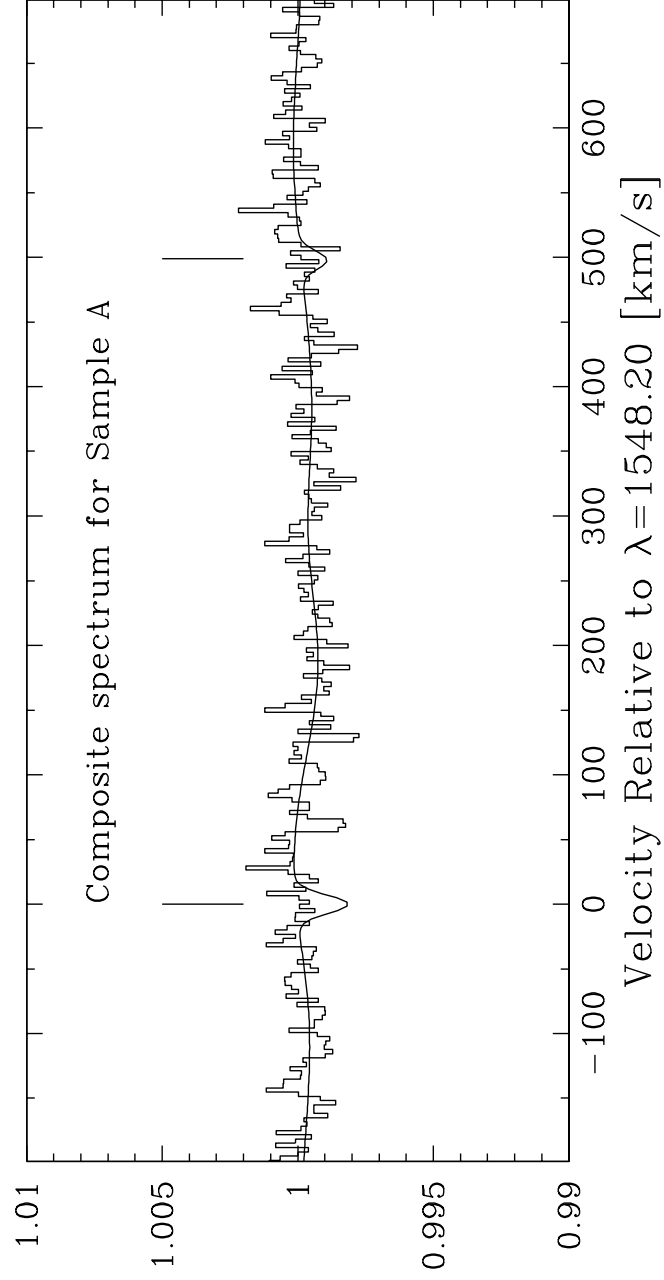


Fig. 3.—

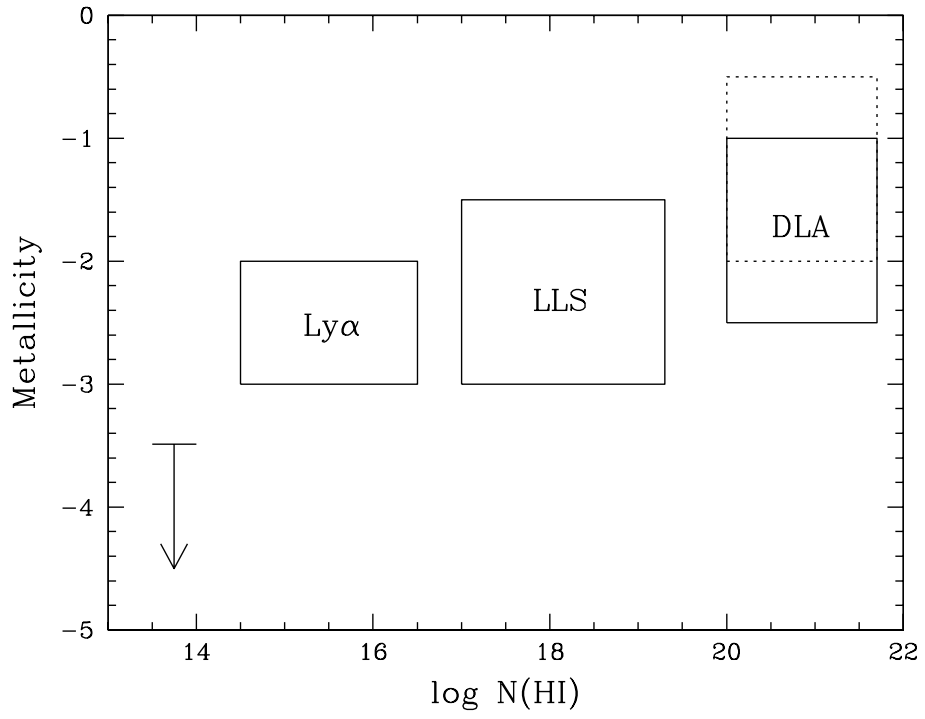


Fig. 4.—

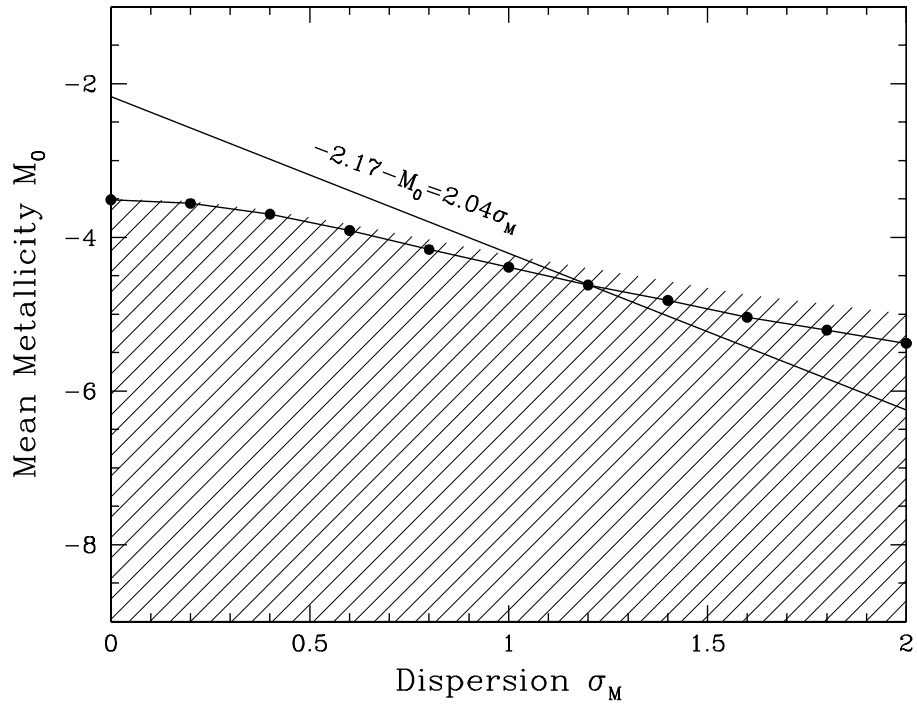


Fig. 5.—